Design for Additive Manufacturing

Oskar Mjelde Mork

Tobias Søtorp Frebrich

Bachelor's thesis in Mechanical Engineering

Bergen, Norway 2024

Western Norway University of Applied Sciences

Design for Additive Manufacturing

Oskar Mjelde Mork

Tobias Søtorp Frebrich

Department of Mechanical Engineering and Maritime studies

Western Norway University of Applied Sciences

NO-5063 Bergen, Norway

IMM 2023 - 05

III

Høgskulen på Vestlandet

Faculty of Technology, Environmental and Social Sciences

Department of Mechanical Engineering and Maritime Studies

Inndalsveien 28

NO-5063 Bergen, Norge

Norsk tittel:	Design for additiv tilvirkning
Author(s), student number:	Tobias Søtorp Frebrich, 597710
	Oskar Mjelde Mork, 674940
Study program:	Mechanical engineering
Date:	05 - 2024
Report number:	IMM 2024-M32
Supervisor at HVL:	Saeed Bikass, Associate Professor
Assigned by:	Bergen Engines, HVL
Contact person:	Saeed Bikass
Number of files delivered digitally:	1

Preface

This bachelor thesis is written at the Department of Mechanical Engineering and Maritime Studies at Western Norwegian University of Applied Sciences (WNUAS) and was conducted in cooperation with Bergen Engines. It was authored by students of the mechanical engineering program, under the supervision of Associate Professor Saeed Bikaas.

Special thanks to Associate Professor Saeed Bikaas for his outstanding guidance and valuable advice throughout this thesis. We are extremely grateful for your support and expertise which was crucial to the successful completion of our work. Additionally, we would like to thank the Bergen Engines team for facilitating the case study and providing valuable insight into their operations. Many thanks to Sjur Herheim, Vidar Natås and Hallvard Blindheim from Bergen Engines for their contribution and engagement in the project.

Abstract

This thesis explores the possibilities of additive manufacturing, aiming to provide a comprehensive understanding by introducing the latest technologies and applying them in a practical case study. The research includes a literature review on the newest advancements in metal 3D printing, examining both its benefits and challenges. Norwegian engine manufacturer Bergen Engines provided genuine engine and production components currently used in their operations today, for the case study.

The case study applies tools such as PTC's Creo generative design to optimize these components for additive manufacturing aiming to unlock geometries and features previously challenging, if not impossible, to produce with traditional manufacturing techniques. This optimization offers advantages such as weight reduction, minimizing material waste, and fewer assembly components. The components were further validated through Finite Element Analysis to validate strength, fatigue resistance, along with other properties to ensure their suitability for use.

Each design includes a theoretical explanation of how they could be produced by different additive manufacturing techniques, along with a cost analysis. The thesis also addresses material selection and necessary considerations for producing the optimized designs trough additive manufacturing. The findings demonstrate that optimizing real world components can unlock innovative geometries with enhanced properties, overcoming the limitations of traditional manufacturing methods. Additionally, the report highlights the ongoing technical and economic challenges that must be addressed for additive manufacturing to become a competitive manufacturing technique.

Sammendrag

Denne oppgaven utforsker mulighetene med additiv tilvirkning, med mål om å gi en omfattende forståelse for produksjons teknikken ved å introdusere de nyeste teknologiene og anvende dem i en praktisk casestudie. Forskningen inkluderer en litteraturgjennomgang av de nyeste fremskrittene innen metall 3D-printing, og undersøker både fordeler og ulemper. Den norske motorprodusenten Bergen Engines stilte reelle motor- og produksjonskomponenter som brukes i deres drift i dag, til disposisjon for casestudien.

Casestudien bruker verktøy som PTC's Creo generativ design for å optimalisere disse komponentene for additiv tilvirkning, med mål om å åpne for geometriske konstruksjoner som tidligere var utfordrende eller umulige å produsere med tradisjonelle produksjonsteknikker. Denne optimaliseringen gir fordeler som vektredusering, minimert materialsvinn og færre monteringskomponenter. De optimaliserte designene ble videre validert gjennom Finite Element Analysis for å bekrefte styrke, utmattings verdier og andre egenskaper, for å sikre deres egnethet til bruk.

Hvert design inkluderer en teoretisk forklaring på hvordan de kan produseres med forskjellige additiv produksjonsteknikker, samt en kostnadsanalyse. Oppgaven tar også for seg materialvalg og nødvendige hensyn ved produksjon av de optimaliserte designene gjennom additiv tilvirkning. Funnene viser at optimalisering av reelle komponenter kan åpne for innovative geometriske former med forbedrede egenskaper, og overvinne begrensningene ved tradisjonelle produksjonsmetoder. I tillegg fremhever rapporten de pågående tekniske og økonomiske utfordringene som må adresseres for at additiv produksjon skal bli en konkurransedyktig produksjonsteknikk.

Table of contents

List of abbreviations

AM	Additive Manufacturing
BCC	Body Centered Cubic
CAD	Computer Aided Design
DED	Direct Energy Deposition
EBM	Electron Beam Melting
FCC	Face Centered Cubic
FEA	Finite Element Analysis
FEM	Finite Element Method
FoS	Factor of Safety
LEAP	Leading-Edge Aviation Propulsion
PBF	Powder Bed Fusion
PLA	Polylactic Acid
SC	Simple Cubic
SDGs	Sustainable Development Goals
SLM	Selective Laser Melting
TO	Topology Optimization
€	Euro (currency)

1 Introduction

Additive manufacturing (AM), also known as 3D printing, involves the process of joining materials to construct objects from 3D model data, typically by adding material layer upon layer [1]. This manufacturing approach has introduced new possibilities in the production landscape, enabling the creation of complex shapes previously unachievable with traditional manufacturing methods.

AM is a relatively new and inventive method for producing parts and assemblies which has seen rapid growth in recent years. Major manufacturers such as Lockheed Martin, Bell Helicopter and other major companies have implemented the method. Lockheed Martin for example have utilized 3D printing to produce and print complex aerospace parts, such as large titanium domes used in spacecrafts [2]. The technology has also been made available to the hobby enthusiast by companies such as Prusa Research, who offers 3D printers for AM in different scale and sizes. Their printers mainly use Polylactic acid (PLA) a type of thermoplastic filament, offering the user possibility to print self-produced 3D models created in Computer Aided Design (CAD) software [3]. These types of printers can also be well suited for small to medium-sized businesses producing different products.

1.1 Motivation

In recent years, the motor industry has shown a growing trend of outsourcing production for their engines and engine components to countries with lower manufacturing costs, predominantly Asia [4]. This trend is driven by the pursuit of cost efficiency. For companies such as Bergen Engines, the adoption of AM presents significant opportunities to ensure the continuance of production for their engines and components, to be kept within their country of origin. Providing jobs, technological advancements, developments of engineering expertise and influence on the transition towards sustainability or “the green shift” [5].

The motivation for this thesis is driven by the authors' interest in AM and Bergen Engines' desire to explore the possibilities with AM and how they can implement this into their production. The manufacturing method has significant advantages but also presents challenges that we wish to explore.

1.2 Objective

The objective of this Bachelor thesis is to investigate the design opportunities and benefits presented by AM technologies. The study will concentrate on four practical case studies from Bergen Engines, focusing on real problems encountered with their engine components and tools.

The analysis will highlight the advantages and address the challenges linked to the application of CAD software and Finite element analysis (FEA) in AM. In addition to utilizing these technological tools, researching literature about the newest technologies, materials, and methods within the field of AM, will be important to further improve case solutions. This approach aims to provide an examination of how these tools and methods can be leveraged to improve design, efficiency, and problem-solving within the context of the case studies.

1.3 Problem statement

How can Creo Generative Design and AM be utilized to enhance the design, weight, and minimize material waste in the production of engine and production components? This question forms the core of several key aspects of this thesis. Through the application of Creo Generative Design and proper material selection we anticipate a reduction in weight, while maintaining desired structural integrity. By

integrating AM, we aim to unlock structures and geometries that were beyond the reach of traditional manufacturing techniques.

1.4 Bergen Engines

Bergen Engines is a Norwegian engine manufacturer that builds medium speed liquid fueled and gas fueled reciprocating engines for marine and land-based operations. Their engines are used in various application from propulsion engines for the Royal Norwegian Navy to large scale land-based operations, such as the largest power plant currently powered by multiple Bergen engines, producing effect up to 200MW [6]. All Bergen engines are built and manufactured at their production facility at Hordvikneset near Bergen in Norway [7].

2 Literature review

This chapter provides a review of recent advancements in AM, focusing on emerging technologies and their applications in enhancing design and production efficiencies. It sets the stage for exploring detailed case studies in subsequent chapters and investigates key considerations that should be considered when optimizing designs for AM.

2.1 Manufacturing technologies

Metal AM has in recent years taken its place in our industry and has become a more valid option for manufacturing than ever before. With serious advantages within adaptivity and optimization, it comes out ahead of many other processes. Even though many parts are still dependent on a second manufacturing process to fix, for example surface roughness, AM can create shapes and geometry previously impossible that allows for a new era of design.

There are various technologies for the fabrication of complex metal parts. Each technology offers distinct advantages, and each is suited for specific projects and applications. What method is used can vary based on the material properties, part requirements (such as detailing, size and complexity), cost effectiveness, and production speed. Powder bed fusion (PBF) and Direct Energy Deposition (DED) are the two methods most relevant to this thesis.

Powder bed fusion (PBF)

There are a few different PBF methods, but they all work under the same principles, that a high energy beam, a laser (in Direct Metal Laser Sintering & Selective Laser Melting) or an electron beam (in Electron Beam Melting), is used to melt or sinter metal particles. The metal particles are distributed in even layers a to create a smooth surface, a “bed”, and then melted or sintered layer by layer by the high energy beam. This gives a supportless part as the powder bed acts as a support during the creation of the part.

Selective Laser Melting (SLM) creates parts with excellent surface smoothness and with nearly complete density [8]. This is highly sought after in the cases we have, as these are high performance parts, that need a homogenous structure with as few pores as possible.

In an investigation comparing the two methods SLM and EBM were performed by Rafi et al. [9] on Ti64 alloy samples, it was shown that there is a substantial difference in tensile yield and ultimate stress values for the two different manufacturing methods. It is worth mentioning that this investigation might be outdated, since it was undertaken 10 years ago, and technology has come a long way in AM since then.

Table 1 - EBM vs SLM manufacturing strength [9]

Method:	Yield stress [MPa]	Ultimate strength [MPa]	Strain at break (%)
EBM (vertically built and machined)	869	928	9.9
SLM (vertically built and machined)	1143	1219	4.89
EBM (horizontally built and machined)	899	978	9.5
SLM (horizontally built and machined)	1195	1269	5

From *Table 1* we see that the stress between the two methods varies from 30-33%, which points to SLM as being the superior alternative for parts in a high stress environment.

Printing Accuracy for SLM

The standard accuracy given by Materialise for their performance materials is DCGT 6 of DIN EN ISO 8062-3 for dimensions between 0.5 and 30mm [10]. This counts for all materials discussed in this thesis marked with "– Performance" as can be seen in *Table 8* and *Table 10*. This gives us a tolerance of ±0.2mm and is an important factor to consider when manufacturing. This standard applies to their SLM manufacturing method and shows that SLM can produce accurate and detailed parts.

Direct Energy Deposition (DED)

Direct Energy Deposition (DED) is an AM process that uses metal as feed (either as wire or powder form) and a laser to fabricate parts on a scaffold or building plate. A nozzle on a multi axis system is used to deposit the material. The method has many different use areas and can be used to create both large and small parts, or repair broken parts. DED encompasses many different AM methods.

Rapid Plasma Deposition (RPD) is a technology within DED patented by Norsk Titanium. It is a method where titanium wire is precisely melted in an argon gas environment while highly monitored. It is a process said to have superior metallurgy which implies material properties on the same level as forged materials, a strong and consistent microstructure, and no lack of fusion in the layers. They can create decently sized objects all the way up to 900 × 600 × 300mm. The layer dimensions are significantly larger than some of the other methods, while having a height of 3-4mm and width of 8-12mm. The technology mainly uses titanium, but is applicable to nickel alloys, tool steel and stainless steel [11].This method is ideal for production of many parts rapidly, but not that great for fine detailed geometry, and would need comprehensive after treatment.

Layer cavities

All the AM methods in principle create the part in layers. These layers create an uneven surface, some more than others. This is an important effect to think about when creating high precision parts that needs to be accurate. To make sure the surface turns out even after machining, it is

important to optimize the parts with this in mind, so the part will end up with an even surface. This is visualized in *Figure 1*.

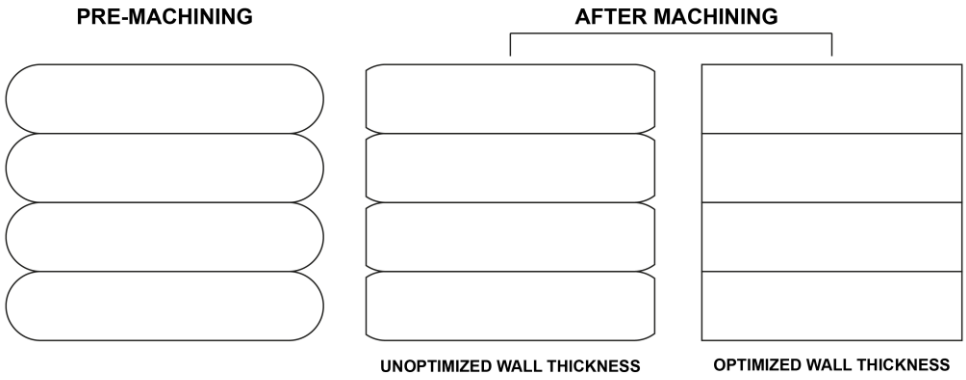

Figure 1 - Optimized/Unoptimized wall thickness.

2.2 Materials for AM

Titanium grade 5 - Ti6Al4V

Titanium alloy is an ideal material for printing because of its cleanliness and high utilization rate in processing. It can be used to create parts with complex shapes with various AM methods like SLM and DED [8]. Titanium alloys are used for many different purposes, everything from aerospace, automobile, and biomechanical industries [12].

There are many titanium alloys used in AM. Materialise, writes about the material, and how to design parts with it [13], [10]. For performance grade material the minimum wall thickness is 0.5 mm, but it may vary depending on the parts geometry, and they recommend 2mm to create features that can be considered structurally sound. They recommend a building angle of no more than 45°, to ensure better and smoother surfaces. Materialise only offers powder bed manufacturing methods, specifically SLM, which is not optimal for some designs, as holes must be created to remove the powder from hollow sections. If this is to be the case, they recommend the holes to be at least 2mm in diameter.

Their recommendations are specific to their manufacturing methods and machines and might not be the standard for every producer. They still present valid points and give us a good baseline for designing our parts.

Custom 465 - C465

Custom 465, also known as C465 is a precipitation hardening stainless steel (PHSS), with high strength and corrosion resistance [14]. C465 is heat treatable and its tensile strength varies from 1034 MPa to more than 1724 MPa depending on what aging treatment is used. The ASTM B117 is a standard practice for operating salt spray and evaluate corrosion resistance of metallic materials and coatings. Exposure to 5% neutral salt spray at 35°C per ASTM B117 resulted in no corrosion after more than 2.000 hours of exposure [15].

The stainless steel is used in various industries today, within aerospace, surgical instruments (scrapers, cutters, and suture needles), in deep-hole drilling operations where driveshafts have proven to last for 1.500 hours more than previously used metals (EN30B or 4330V), and in the automotive industry as

suspension coils and engine valve springs. It is considered a good corrosion resistive replacement for steels like 300M and AISI 4340, and a higher strength replacement for 15-5, 17-4 and 18-8 stainless steels [15].

42CrMo4 (1.7225)

42CrMo4 is a high strength martensitic steels containing chromium, molybdenum and manganese increasing its hardness, strength, and hardenability. It is used in various industries for its high toughness, fatigue strength and impact resistance. Some industries are aerospace, automotive, and oil and gas. The parts usually created with this steel are gears, spindles, shafts, and jigs. The steel can be hardened by cold and hot working or quenching and is easily machined [16].

Parts in 42CrMo4 can be manufactured trough PBF both trough EBM and SLM [17]. In an investigation of the properties of steel after EBM manufacturing it was found it could be created with an ultimate tensile strength between 800-1200 MPa depending on build direction and treatment [18]. These values are the same as other datasheets found on the material [19], which tells us the AM capabilities of this material are excellent.

Case-Hardening Steel 20MnCr5 (1.7147)

20MnCr5 has the unique ability to case-harden, which gives it very high hardness and wear resistance. It has a small grain size which gives it high fatigue strength and good ductility [20].

20MnCr5 can be case-hardened and welded, which makes it a very versatile steel and popularly used in the production of engineering parts, such as gears, shafts, axles, and rods. The case hardening steel 20MnCr5 can be successfully processed in a PBF method shows an investigation on the topic, from the HTM Journal of Heat Treatment and Materials [21].

2.3 Weight reduction

In today's world, where efficiency and sustainability are becoming increasingly important, reducing weight plays a crucial role. Traditional manufacturing methods often result in excessive material use, leading to heavier and bulkier final products. However, AM offers opportunities to decrease component weight significantly while ensuring structural integrity [22].

The aviation industry recognizes these advantages and has embraced AM to produce lighter aircrafts. Lighter planes can carry more passengers, handle larger payloads, achieve longer ranges, exhibit better maneuverability, and require simpler maintenance. [23]. There are numerous successful examples of additively manufactured airborne components. For instance, General Electric has innovatively produced a fuel nozzle for the Leading-Edge Aviation Propulsion (LEAP) engines using AM. This approach consolidated 20 separate parts into a single component, produced on one machine, reducing the weight by up to 25% compared to its conventionally manufactured counterparts. [24]. *Figure 2* displays the fuel nozzle produced with AM.

Figure 2 - General Electric's fuel nozzle produced with AM [24].

Parts that are manufactured using traditional techniques tend to be heavier, which can lead to higher fuel consumption during operation [25]. On the other hand, a lightweight design created through AM can help reduce CO2 emissions, aligning with the United Nations Sustainable Development Goals (SDGs) of Responsible Consumption and Production [26].

To achieve weight reduction, designers should consider removing unnecessary material and utilizing lattice and gyroid structures. This requires rethinking traditional design constraints tied to machining or molding, etc. Designers aiming to optimize weight should focus on the essential elements required for the component to function and eliminate excess material without sacrificing strength and functionality. By incorporating lattice and gyroid structures in 3D printing, it may be possible to create robust, lightweight components and optimize stress distribution, potentially achieving an advantageous strength-to-weight ratio [22].

2.4 Lattice structures

One of the advantages of AM is the possibility to create internal structures with great strength to weight ratio. These structures are called lattice structures. There are endless designs for lattice structure, with many different purposes.

One of the most famous lattice structures is created by nature itself, and it is in fact the honeycomb found in beehives (*Figure 3*). The act of mimicking natures design is called biomimicry, and its purpose is to learn design rules from systems created in nature and use this to our advantage in engineering designs [27]. Honeycombs for example is a very strong lattice that specializes in maximizing storage area for its honey, while at the same time having a strong and stable structure to maintain a huge hive. The honeycomb has become a staple lattice structure and is a widely used biomimicry in human design. It has many different applications, some of them being: Vertical insulating bricks [28], wall panels [29], or just cardboard boxes.

Figure 3 - Honeycomb lattice structure, picture created with ChatGPT.

In a performance evaluation of different lattice structures by Johannes Scheider [30], it is found that the lattice structure with the best stress distribution, and great stiffness and strength is the gyroid structure. With only the simple cubic structure (SC) outperforming its stiffness and strength. The performance evaluation tested Octet and Kelvin truss-lattices, Gyroid shell-lattice, and SC, body centered cubic (BCC), and face centered cubic (FCC) plate-lattices. All structures had similar relative density and were tested both with experiments and FEA. The gyroid structures uniform stress distribution and no localized stress peaked, makes it an optimal contender for any parts.

2.5 Fatigue

Fatigue is a type of structural failure that typically occurs in machine components or structures subjected to dynamic and fluctuating stresses. This type of failure can manifest even at stress levels significantly lower than those required to breach the tensile or yield strength of the material in static loads. The emergence of fatigue is often associated with prolonged periods of repeated stress or strain cycling. It is the primary cause of failure in metals, accounting for up to 90% of all metallic failures. Fatigue failure can be catastrophic, often occurring abruptly and without any prior warning, potentially leading to dangerous scenarios that could result in severe structural, environmental, or personal damage [31].

Fatigue is a gradual process that occurs over time and does not involve large visible deformations, making it challenging to detect. One tragic example of fatigue failure is the Alexander Kielland disaster. Alexander L. Kielland was a drilling platform that capsized in the Ekofisk oil field in March 1980, killing 123 people. The investigation report concluded with the fact that a fatigue fracture in a support structure to one of the platform's legs had triggered the accident [32].

The fatigue behavior and structural performance of metal parts produced by AM are affected by various factors such as machine settings, build direction, surface roughness, residual stress, and heat treatment. One major concern in AM is the variability in microstructure and the defects produced, which are heavily dependent on the manufacturing process parameters. The microstructure of such parts is influenced by a range of machine settings and the thermal history during fabrication, including laser settings and temperature changes. Although these aspects affect grain size and defect distribution, the cooling rate remains the primary determinant of the microstructure's evolution [33].

Research has demonstrated that the most frequent causes of fatigue cracks in AM parts are pores from trapped gas, typically spherical, and irregularly shaped voids resulting from insufficient sintering during the printing process [33]. *Figure 4* displays the formation of irregular, spherical and open pores, a typical defect in SLM produced parts.

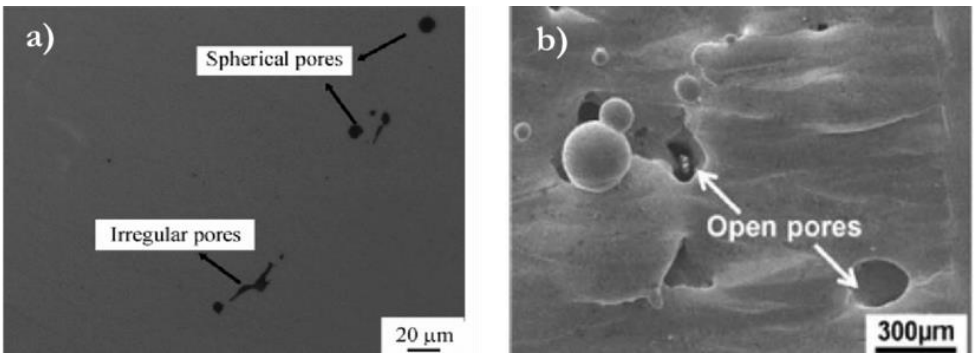

Figure 4 - Typical defect of SLM produced parts [34] .

Several studies have been conducted to determine the effect of build direction on fatigue strength. However, the results of these studies have been inconsistent. While some studies show that build direction has a significant impact on fatigue strength, others show no substantial effect.

One extensive study conducted by Kovulchak et al. examined the effect of build direction on fatigue and mechanical strength in 3D printed Ti-6Al-4V. The study involved performing fatigue and tensile tests on sample rods cut out from central areas of 3D printed blocks built in the “X”, “Y”, and “Z” directions. The study concluded that the best mechanical and fatigue properties were observed when the direction of the applied stress was parallel to the layer-by-layer structure. This implies that if the build direction is perpendicular to the applied stress, the part may exhibit poorer fatigue and strength characteristics. It is worth noting that electron beam melting was used in manufacturing the titanium alloy blocks used for testing in this study [35].

There are several methods for assessing fatigue life and strength. One method is through static stress analysis using the Finite Element Method (FEM) to evaluate stress concentrations against a specified fatigue limit. Since fatigue damage typically propagates perpendicular to the direction of the maximum principal stress range, analyzing both maximum and minimum principal stresses is important [36]. By doing so, engineers can directly assess how these stresses correlate with the specified fatigue limit to understand and predict fatigue behavior. This analysis helps in identifying regions where the stress exceeds the material's capacity to withstand repeated load cycles, thereby pinpointing potential failure sites for further investigation and design optimization [37].

3 Method

This chapter presents the methodologies, software applications, and techniques employed in this thesis, which establishes the groundwork for the subsequent analysis presented in the case studies chapter.

3.1 Collaboration with Bergen Engines

This thesis investigates modern advancements in manufacturing through a case study conducted in collaboration with Bergen Engines. The company extended support by supplying case-specific 3D files and facilitated a comprehensive understanding of their operations. An initial session was organized with Bergen Engines to glean insights into their corporate ethos, their state-of-the-art production facility at Hordvikneset, and their perspective on integrating AM into their processes.

A visit to the Hordvikneset facility yielded valuable observations about their existing production lines, showcased in *Figure 5*, and provided a tangible context to their current product offerings, which include complex machinery components as pictured in *Figure* 6. Their facility boasts some of the most sophisticated machining technologies available today, as demonstrated by the equipment and machinery in operation during the site tour.

Figure 5 - Inside Bergen Engines' facility, two technicians surface treat one of Bergen Engines colossal engine blocks.

Bergen Engines is at the forefront of innovation, investigating the integration of AM to enhance their production capabilities. Communication with Bergen Engines was maintained through a balanced mix of interactions, including a face-to-face meeting at their production site, which allowed for a direct experience of their operational environment, supplemented by digital meetings and email correspondence to ensure continuous engagement and information exchange.

Figure 6 - *Detailed view of Bergen Engines' advanced production line, featuring a worker operating the MACTURN 550 machine.*

3.2 Topology optimization

Topology optimization (TO) is a simulation-driven design method commonly used in the creation of physical systems and mechanical structures. It is particularly useful for manufacturers as it provides an advantage in designing complex parts. Determining the best design for a structure can be difficult, as it needs to withstand the loads it will be exposed to, while not using excess material. Using physics and mathematical methods, TO optimizes the distribution of material within a defined domain to create the most efficient design. This method takes a 3D design space and removes any unnecessary material to achieve the desired outcome. When utilized in AM, TO has several advantages. It enables the creation of structures that were previously difficult for humans to conceptualize, and these structures provide benefits such as weight reduction and minimized material waste. The complexity of these structures means that they would be challenging, if not impossible, to produce using traditional manufacturing methods. Therefore, TO is particularly well-suited for AM. [38], [39]. *Figure* 7 Illustrates the TO process.

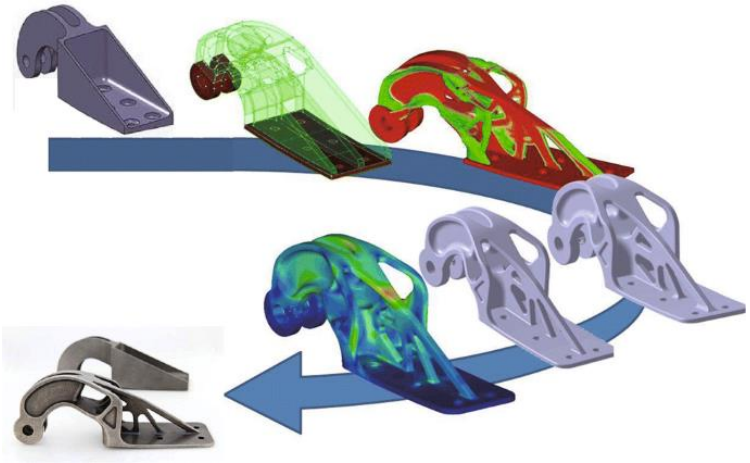

Figure 7 - *Topology optimization process* [40].

Generative design in Creo

Bergen Engines has shared some cases with us where we'll be redesigning complex machine components. To achieve a reduction in assembly components, weight reduction, and reduced material waste, we plan to use TO in our designs. There are several software options available for TO optimization, we will be using Creo Parametric's generative design. This technology has only become available in recent years, and it builds on the foundation of TO while offering new functionality in design optimization. In generative design, the user selects a design goal for the optimization. The user can choose to maximize stiffness by selecting a target volume (in %) or minimize mass by specifying a safety factor. The program will then minimize the mass of the geometry while removing all unnecessary material to meet the specified safety factor. [41].

Figure 8 - Part optimized by Creo's generative design.

Where generative design really excels is in its option for setting one or multiple geometric constraints for the optimization study. These geometric constraints are specifically targeted towards AM and involve options like build direction, which is a constraint who helps in reducing the amount of support needed for 3D printing. The user specifies the direction the geometry will be 3D printed and the value of the critical angle. Critical angle is the maximum angle with respect to the print direction at which supports are not needed [42]. Build direction can have a significant impact on the mechanical properties of the design, dependent on the printer type and in which material it is printed. Several studies have investigated the effect of build direction on the mechanical properties of parts produced by PBF methods. While the results vary, it is generally recommended to align the build direction parallel to the applied stress. As a build direction perpendicular to the applied stress can result in weaker mechanical properties and poorer fatigue characteristics [43], [35] and [44]. Other main design criteria's available are parting line, linear extrude, symmetry, material spreading and minimum crease radius.

Parting line – Is a manufacturing constraint which is mostly used in casting and forging methods. Parting line refers to the edge or line where two parts of a mold meet. Creo generative design provides the option for choosing where this point should be, the parting line in molds is crucial because it can influence the ease of mold opening and part ejection, thereby affecting the manufacturing efficiency and the quality of the final product. Correctly identifying the parting line helps predict and minimize potential defects such as weld lines and air traps that are common in areas near the parting lines. For 3D printing one can efficiently create molds in Creo generative design and use these molds to produce the cast parts.

Linear Extrude – Is a manufacturing constraint which can be used for parts that will be extruded or machined. In generative design linear extrude can help in creating uniform or graded structures to withstand the specific loading conditions while minimizing material usage. Linear extrude help identify

optimal extrusion paths which optimizes the structural integrity of the part, while also simplifying manufacturability.

Symmetry – A geometric constraint which builds planar, rotational or both types of symmetry. The constraint creates symmetric structures regardless of asymmetric loading in the study. By incorporating symmetry into the design one can significantly reduce computational time in the optimization process and it can also lead to more aesthetically pleasing designs.

Material Spreading – A geometric constraint which controls the spreading of the material in the part. The spread value is specified by the user, choosing what % the material is to be spread from 0 -100%. Increasing this value leads to a design with fewer thick and solid areas, and more thin walls and support structures. Material spreading is relevant to AM as it directly influences the density and distribution of material within the design space. This constraint is particularly important for parts which have internal geometries which are to be optimized, such as parts with lattice or honeycomb structures, which cannot be produced by traditional manufacturing methods.

Minimum crease radius – A geometric constraint which can be used to smooth out the geometry and reduce the occurrence of thin, web-like structures in the design. It ensures that all surfaces maintain a curvature with a specified minimum radius. For 3D printed parts, ensuring smooth transitions and avoiding sharp corners is crucial to maintaining structural integrity. The minimum crease radius constraint helps in smoothing out the geometry, reducing stress concentrations and improves the appearance of the part. In AM sharp angles can lead to material accumulation or defects. By setting a minimum crease radius, one can influence more uniform stress distribution and reduce the likelihood of failure [45].

3.3 Lattice design

Creo Parametric offers tools for designing lattice structures, that can be highly beneficial for AM applications. Creo along with literature reviews and scientific articles, were the main research and investigation methods we used for lattice structures. The goal of looking at lattices was, if beneficial to our design, to implement lattice as internal structures for strength, or for supporting other designs with critical support angles.

When lattice is created in Creo, there are made cells for a given size as seen in *Figure 9*. Depending on how many cells are created there are three different types of lattice representations [46].

Full geometry - If the number of cells is less than 7.000, a full geometry model can be used in Creo simulations. The whole structure in this can would be transferred to Creo Simulate

Simplified lattice - If the cell count ranges from 7.000 – 24.000 a simplified lattice model can be used for structural simulations. If this is the case, the midplane of the thin 2.5D lattice es extracted and a shell model is built by Creo.

Homogenized - If the cell count is larger than 24.000 it is created and used a homogenous representation from Creo. This is a method where material properties are estimated and simulated as a homogenous structure.

A 3D gyroid lattice structure was constructed in Creo, using the lattice function, with 0.5 [mm] wall thickness and 16.2 × 16.2 × 16.2mm cell size. It was tried to run simulations on it, but the 3D formula driven lattice structures (inc. Gyroid, diamond and primitive) in Creo parametric struggles with simulations as they won't mesh properly. Creo does not construct bodies with formula driven lattices, but rather uses a formula to define and illustrate the lattice cell shape. This makes formula driven lattice structures hard to work with in Creo, as there is no good way to approximate weight, density or run simulations.

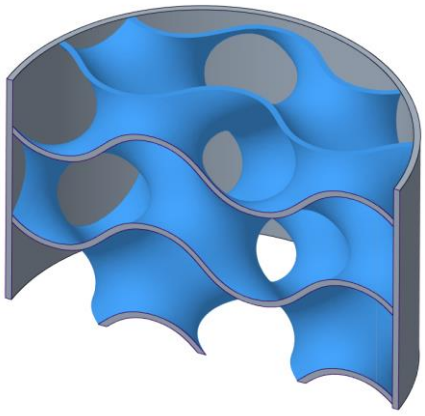

Figure 9 - Gyroid structure created in Creo; Cell scale: 0.5, Cell size: 16.2 x 16.2 x 16.2 [mm], Wall thickness: 0.5 [mm]

Meshing has also been an issue, so the main resource and usage for lattice structures in this thesis are literature work, as it is hard to create simulations for the most stable and durable lattice structures, as tiny imperfections make them unable to mesh.

3.4 Finite Element Method (FEM)

There are a variety of analytical methods that engineers can use to solve structural problems, such as calculating the deflection of beams and stresses that they are subjected to. However, complex structural problems are often not solvable with these methods, due to the intricate geometry, material, or loading conditions involved. FEM is a numerical technique that is particularly adept at solving these complex problems with a high degree of accuracy.

FEM software is widely used in all major engineering industries. It can be used to analyze a wide range of solid mechanical problems, including static, dynamic, buckling, and modal analyses. It can also be used for fluid flow, heat transfer, and electromagnetic problems. For this thesis we will focus on how it applies to static linear-elastic stress analysis. The goal of a static stress analysis is typically to calculate the stresses, strains, and displacements within the solid part. For a solid 3-dimensional part FEM approaches the problem by splitting the body into several small elements that are connected at nodes, a method called discretization and the collection of nodes and elements are called mesh. Discretization is useful because when applied, the equilibrium requirement used in analytical methods, now only needs to be satisfied over a finite number of discrete elements, instead of continuously over the entire body of the part. The powerful software then calculates stresses, strains, and displacements within each element. Choosing proper element size and element type is crucial for the accuracy of the study and has a great effect on computational time [47].

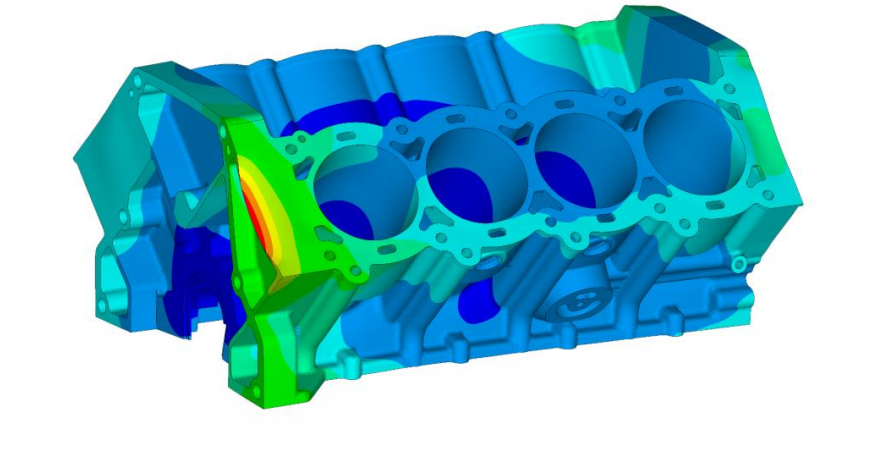

Figure 10 - Illustration of Finite Element Analysis on an engine block [48].

For the case studies involving Bergen Engines, we will be employing FEM to calculate stress, strain, and deformation on our optimized designs. This step is essential to ensure that our optimized designs can withstand the loading conditions they would be subjected to, with their designated material. Moreover, we will compare the original designs with our optimized designs to demonstrate how generative design can create efficient geometric designs suitable for use in their Bergen Engines motor or production processes. For our structural analysis, we will be using Ansys Mechanical software, which is compatible with Creo Parametric and is one of the world's leading FEA software used by engineers. We will also be utilizing Creo's inbuilt "live simulation" to carry out FEA.

3.5 Cost estimation

Numerous companies offer 3D printing services, providing customers with the ability to print 3D models using various materials and manufacturing techniques. Potential customers can upload their CAD models securely and confidentially to receive an instant price estimate for printing their parts with the most suitable manufacturing process for their chosen material. These companies use software to provide instant price estimates, although in cases involving complex 3D models or custom materials, the software may require manual intervention by an engineer for accurate pricing. In this thesis, to approximate the cost of designs optimized for AM, we have utilized these services, obtaining both instant and manually assessed price estimates by engaging with the suppliers. These price estimates also include post-processing options such as surface finishing and potential heat treatments [49], [50] and [17].

Furthermore, the cost estimate for the original parts was provided by Bergen Engines in NOK and has been converted to Euros using the exchange rate as of May 15, 2024. This information will be used to compare the costs of AM to traditional manufacturing, providing valuable insights into the benefits and drawbacks of AM.

4 Case studies

This chapter presents a series of case studies, the cases are provided by Bergen Engines. These cases involve actual engine and production components that are currently used by Bergen Engines in various applications. The purpose of this case study is to enhance genuine components for AM trough a practical approach, and demonstrate the advantages associated with AM, while also addressing the challenges and difficulties that it presents.

4.1 Case definition – Case 1

Case 1 is a redesign for a swing arm (*Figure 11*) presented by Bergen Engines, with a focus on optimizing it for AM. Currently, the swing arm is manufactured through traditional machining methods, leading to significant material waste for such a small component. The swing arm assembly consists of multiple components illustrated in *Figure 12*. The objective is to optimize the swing arm without necessitating alterations or adjustments to the assembly components.

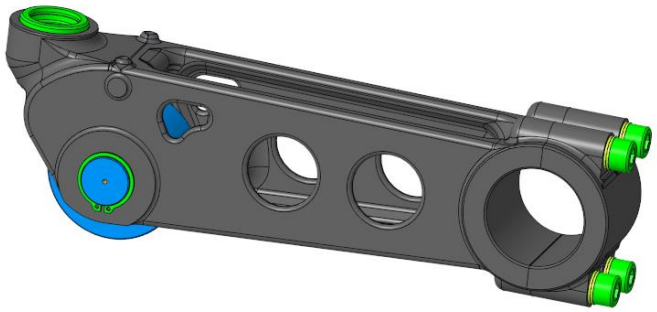

Figure 11 - Case 1 the original swing arm.

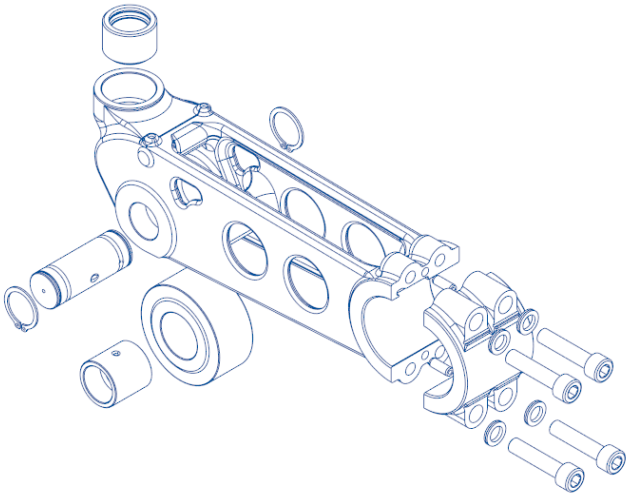

Figure 12 - Assembly of case 1.

During operation, the swing arm is exposed to an external force from a push rod, the force from the push rod acts directly on to the impact cup. Under normal operation the magnitude of this force has been measured to 15 kN. However, under max operational conditions the force has been measured to 29 kN. The external force is highlighted in *Figure 13*. The resulting force generated by the push rod is a consequence of the thrust exerted on the cam roller by the camshaft. As the cam roller thrusts upward,

directed towards the impact cup, the resulting force is transmitted through the push rod. The contact force originating from the cam roller shifts during operation, and the impact point is not consistent. For analysis purposes. we assume a sector of 60° for the impact point, as illustrated in *Figure 13*. The swing arm is clamped to the VVT shaft, this clamping effectively restricts both horizontally and vertical movements, while allowing free rotation of the swing arm by a rotary bearing. The point of the boundary conditions is designated by the blue markings in *Figure 13*.

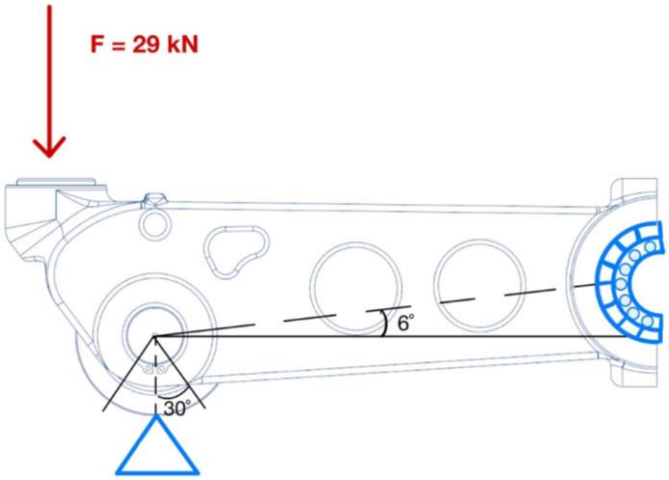

Figure 13 - Load and boundary conditions for the swing arm.

The original swing arm is constructed from a ductile cast iron, specifically grade GJS-500, in accordance with the EN standard. Bergen Engines has specified a safety factor of 1, which will be used to evaluate the redesign in the Finite Element (FE) results. The conditions for this case are detailed in *Table 2*.

Table 2 - Design conditions, Swing arm

Conditions		
Load type	Dynamic, load is applied as the cam roller is thrusted up into the impact cup.	
Load Magnitude	Max load of 29 [kN] under operation	
Support	Swing arm is fixed around VVT shaft, enabling rotation around a fixed axis.	
Material	Cast iron EN-GJS-500 with material properties	
	0.2% Yield Strength	320 [MPa]
	Young Modulus	178 [GPa]
	Density	7000 [kg / m^3]
	Poisson's ratio	0.28
Safety factor	1	

When optimizing the swing arm, there are specific geometric limitations we must adhere to, to ensure that the arm functions as before. This is essential so that no adjustments are needed to the other components that interact with the arm. These limitations include:

- The dimensions of the clamp attachment to the crankshaft must be preserved.
- The diameter at insertion point for bushing bearing (for the cam roller) must be preserved.
- The dimensions for the impact cup must be preserved.
- The arm features internal oil channels that need to be maintained, their placement can be changed, but they must be present.

In summary, the objective of the first case study is to optimize the design of the swing arm through the use of generative design, which is a powerful tool that can aid in weight and volume reduction while maintaining the structural integrity of the swing arm. The optimized design should be adapted for AM, and an exploration of suitable materials for metal printing should be conducted. Additionally, the new design should be compatible with the assembly parts and ensure proper conveyance of lubrication through internal oil channels. The final design of the swing arm should effectively demonstrate the benefits of AM, such as complex geometry and minimized material usage leading to decreased material waste when compared to traditional production methods.

4.2 Case definition - Case 2

Bergen engines have assigned the task of redesigning a spindle. They want a spindle that has a wider section along its body for easier assembly of the gas admission valve for their engine, as it today has multiple smaller parts which makes for an intricate assembly. The design challenges come down to having a weight increase of no more than 10% if possible, while achieving structural strength comparable to the original spindle (*Figure 14*).

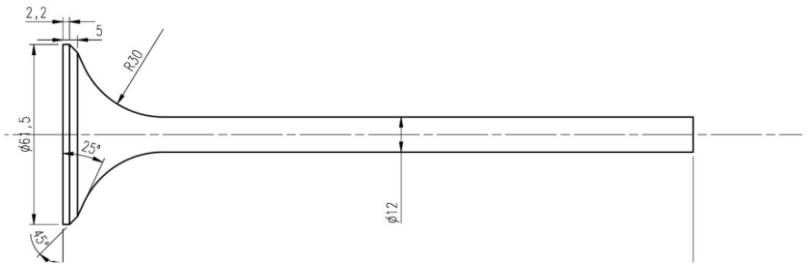

Figure 14 - Drawing of original spindle design.

The outer shape of the spindle is determined by Bergen Engines and is given by drawing (*Figure 15*). Within the dotted lines, the spindle should be massive. All the hollow sections of the spindle should at least have an outer wall of 2 mm, if it is possible within the other limitations given. This means that if the weight limit can't be reached, the walls could be thinner if it meets the structural strength criteria. Other design conditions can be found in *Table 3*.

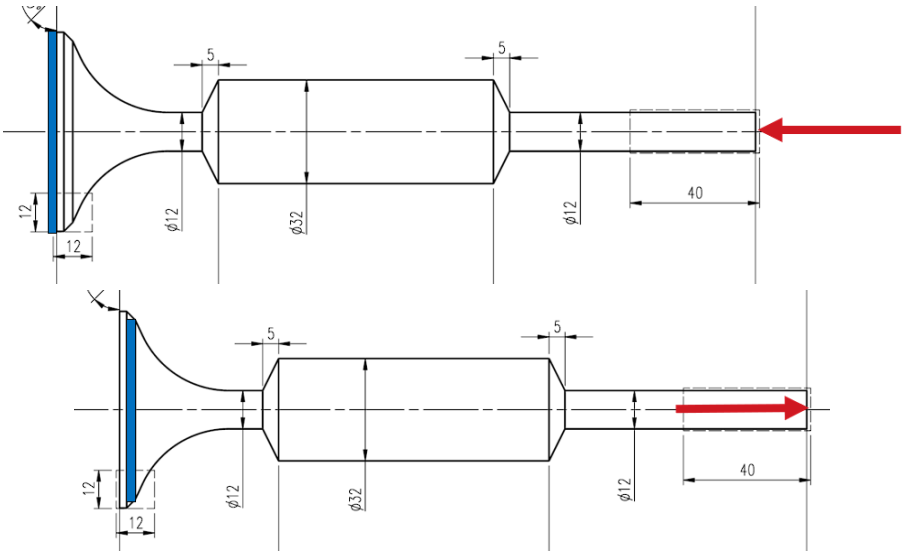

Figure 15 - Parameters for spindle redesign and forces.

Table 3 - Design Conditions, Spindle

Conditions		
Load Type	Dynamic, Tensile and compression	
Load Magnitude	5000 N, shown by red arrows	
Support	Blue area of figure, switching between the angled surface, and the surface normal on the spindle	
Desirable properties	- 3D-printable - Able to harden. - Corrosion resistant	
Previously used Material	X45CrSi9 ref EN10090 with material properties:	
	0.2% Yield Strength	700 [MPa]
	Young Modulus	210 [GPa]
	Density	7700 [kg / m^3]
	Poisson's ratio	0.3
Factor of Safety (FoS)	Not specifically given, but if the spindle can maintain deflection and stress within the elastic boundaries of the chosen material, then it is strong enough.	
Geometric limitations	Within dotted lines in figure: solid Everywhere else: min. 2mm thick wall if possible. The outer shape is given by drawings.	
Weight	Up to 110% of original part	
Manufacturing Processes	3D-print > Fine machining > Hardening if needed.	

Simulations shown in *Figure 16*, conducted by Bergen Engines, on the hollow spindle with no internal structures, reveals a deformation of 0.08 mm under compressive stress and tensile stress, and a peak Von Mises stress value of 282.6 MPa. The objective is to minimize these values, comparable with the original design, within the weight limit.

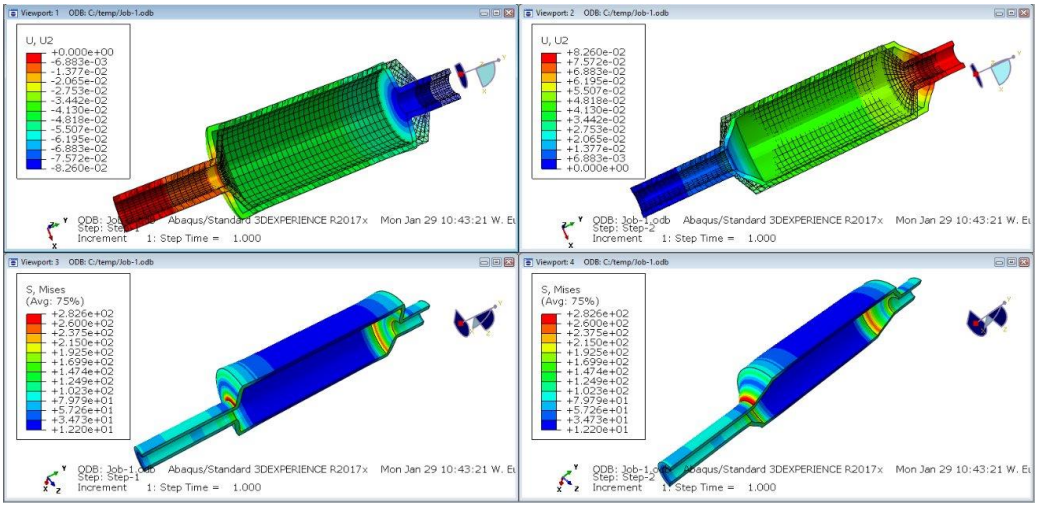

Figure 16 - Hollow spindle simulations. Compression (Right side), Tensile (Left side).

When complete, the new spindle should have a design that utilizes the advantages of AM. With AM some solutions involve generative design or lattice structures within the spindle. While AM is the heart of this problem, one should also investigate what other manufacturing processes would be needed, as this part requires low surface roughness, and the AM technology we have today might not be able to do it alone.

4.3 Case definition – Case 3

Case 3 presented by Bergen Engines is an assembly part for one of their camshaft drive systems. The assembly presented is a camshaft extender, including a gear wheel, the arrangement's main function is to operate the camshaft. Currently this arrangement is adapted for machining considerations. The focus in this case will be to optimize the Camshaft extender for AM by reducing its number of assembly components. *Figure 17* displays the camshaft extender with its gearwheel mounted and displays the camshaft extender only.

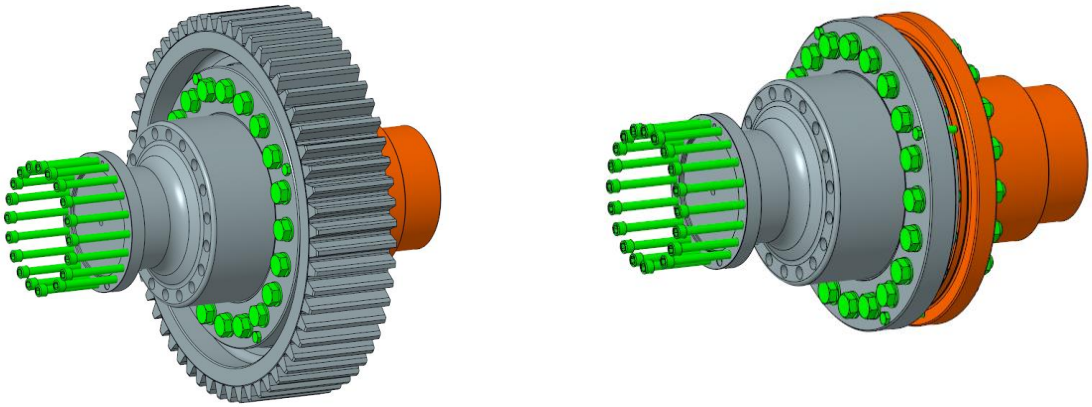

Figure 17 - Camshaft extender without (Left) and with (Right) gearwheel.

During operation the extender transfers the power from the camshaft, flange marked in red on *Figure 17* is for mounting and the extender in grey from *Figure 17* is to simply connect the camshaft. Currently the camshaft extender is in 4 parts, this is only because it is adapted to machining considerations. With AM we see a possibility here to reduce the total number of parts, as we can print some of the assembly

in one part. *Figure 18* show an exploded model of the main components to illustrate the current solution, bolt nut connections are hidden.

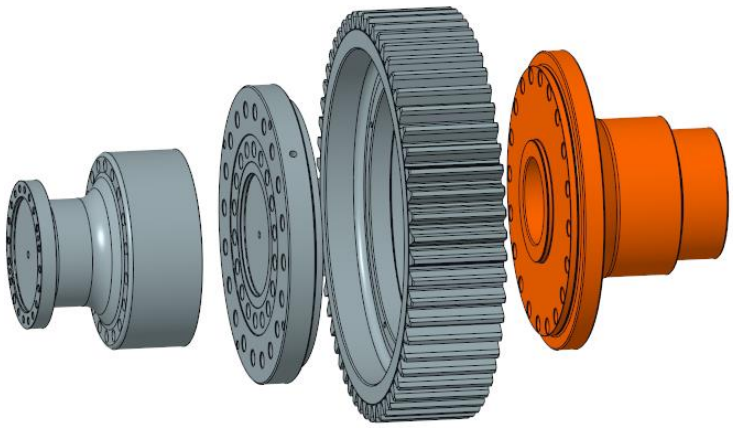

Figure 18 - Exploded model of main components camshaft extender.

Assembly and Load Conditions

The gearwheel is mechanically joined to the camshaft through a bolted flange arrangement. The bolting is tightened with a specified torque of 550 Nm, which corresponds to a calculated fastening load of 137. kN per bolt.

Calculating the bolt preload [51]:

$$T = K \times D \times P$$

Where:

T – torque applied to tighten bold

D – major diameter of the bolt

P - bolt preload

K – nut factor or tightening factor

Table 4 provides standard K values for different bolt conditions*:*

Table 4 – Standard K values

K	Type of bolt
0.2	Steel bolts (with no plating)
0.15	Steel bolts with cadmium plating
0.28	Steel bolts with zinc plating
0.18	Steel bolts with lubrication

For the calculation, Steel bolts without plating are used where K = 0.2 and major diameter of bolt D = 20 mm

$$P = \frac{T}{K \times D} = \frac{550\ Nm}{0.02\ m \times 0.2} = 137.5\ kN$$

In operational conditions, a resistance moment acts upon the gearwheel due to the camshaft rotation, resulting in a torque of 25 kNm transmitted to the camshaft extender. The camshaft itself is constrained at both ends to prevent radial and axial movement yet allows for tangential rotation. The illustration of these forces and the camshaft's boundary conditions are outlined in *Figure 19*.

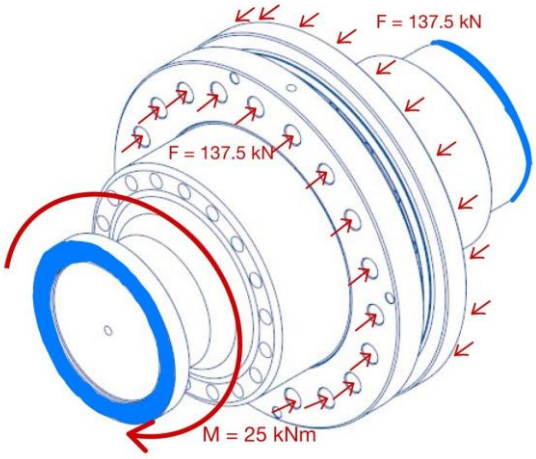

Figure 19 - Illustration of loading and boundary conditions for the camshaft extender.

Materials

The assembly includes components made from materials chosen for their mechanical strengths and durability. The flanges and camshaft extender are constructed from 42CrMo4 steel, while the gearwheel is made from 18CrNiMo7-6 steel, both materials are noted for their toughness and resistance to wear.

42CrMo4 Steel**:** This low-alloy steel is enriched with chromium and molybdenum, enhancing its ability to withstand wear and stress. Its yield strength varies depending on component size; the larger diameter of the flanges results in a lower yield strength compared to the smaller diameter of the extender, though both are crafted from the same steel [52], [53].

18CrNiMo7-6 Steel**:** The gearwheel faces continuous operational stress and is manufactured from this steel, known for its robustness. It undergoes a case-hardening process that includes the addition of

chromium, nickel, molybdenum, and carbon, plus quenching and tempering to create a surface that can endure the intense demands of gear functionality [54]**.** The specific material and mechanical properties for these materials with their respective parts is displayed in *Table 5.*

Table 5 - Material properties, original camshaft extender

Part	**Material**	**Derived from standard**	**0.2% Yield Strength [MPa]**	**Young Modulus [GPa]**	**Density [kg/m^3]**	**Poisson's ratio**
Extender	42CrMo4	NS-EN 10083-1	500	210	7800	0.3
Flange's	42CrMo4	NS-EN 10083-1	390	210	7800	0.3
Gearwheel	18CrNiMo7-6 + QT	EN 10084	650	210	7850	0.3

Geometric limitations:

- The arrangement is installed through a narrow space within the engine block, and the redesigned assembly must not exceed the original dimensions in terms of overall length and width to ensure it fits properly.
- The arrangement must be a two-part assembly surrounding the gearwheel. The fit between the gearwheel and the two flanges is precise, allowing minimal tolerance.
- The external profile of the gear must be preserved to ensure compatibility with the rest of the system.
- The bolting connection between the extension and camshaft section, as well as the flange for mounting, must be preserved.

Design and Safety Criteria: The design will be evaluated against critical safety factors, such as the fatigue limit of 250 MPa and a yield limit of 500 MPa. It's essential to assess whether the flanges can sustain the friction required to transmit the operational torque effectively.

Objective: The current production technique necessitates a four-part assembly; however, AM offers the potential to simplify this by reducing the number of components, minimize material waste, and achieve a lower weight trough structural optimization. The primary objective for the case study is to transform the current four – part assembly into a more compact three-part system, specifically adapted for AM. A secondary objective is to decrease the overall weight of the assembly without compromising its durability and structural integrity. Due to the space constraints for mounting, careful attention must be paid to the dimensions of the gear and extension.

4.4 Case definition – Case 4

The wheel adapter for probing serves as a critical tool in the alignment and positioning of engine components, particularly within the cam bore of the engine. The wheel is placed within the bore of the engine, and then interacts with the machine probe to find the right position/geometry. Today the wheel is too heavy. In Case 4 our objective is to redesign the wheel tool for a lighter weight, but maintaining adequate structural integrity, so that the wheel doesn't warp or bend easily. Other design conditions are found in *Table 6*.

Table 6 - Design conditions, Wheel for probing

Conditions		
Load Type	No loads	
Load Magnitude	No loads	
Support	No specific supports given	
Desirable properties	- Concentric - Low thermal expansion - High precision - Light weight	
Previously used Material	42CrMo4 from standard NS-EN 10083-1:	
	0.2% Yield Strength	500[MPa]
	Young Modulus	210 [GPa]
	Density	7800 [kg / m^3]
	Poisson's ratio	0.3
Factor of safety (FoS)	N/A	
Geometric limitations	Outer wheel diameter: 296mm Inner wheel diameter: 200mm	
Original volume:	0.655 dm^3	
Manufacturing Processes	3D-print > Fine machining > Hardening if needed.	

Figure 20 - Original Wheel for probing.

From *Figure 20* the two red surfaces are the important diameters to maintain on the wheel. These diameters need to have a very precise tolerance and be perfectly concentric, which means it can't be used straight from the 3D-printer, it will need a secondary machining method for creating perfect diameters.

The current design uses 42CrMo4 steel as a material. Although the heat treatment specifics are not detailed, annual inspections by Bergen Engines suggest that the wheel likely undergoes tempering to enhance its durability and mechanical strength. For the new material, aluminum has been considered earlier by Bergen Engines, for its lightweight property, but was dismissed for its thermal properties, which would lead to issues with warping. Therefore, when selecting material for the redesigned wheel, factors such as mechanical strength, durability, and thermal behavior will be critical to consider.

5 Design for AM - results

This chapter presents the findings from the case studies conducted as part of this thesis. It details the process involved in redesigning the components and presents the results of FEA conducted on both the original and optimized parts. Additionally, it provides an overview of the manufacturing processes and costs associated with the optimized parts. These aspects are compared to their original counterpart to evaluate improvements and assess performance enhancements.

5.1 Case 1 - Swing arm

The redesign of Case 1's swing arm focused on optimizing the component for AM and reducing its weight through enhanced structural strength, utilizing Creo's generative design capabilities. Compatibility with existing assembly components and the preservation of internal oil channels for lubrication were also essential requirements.

5.1.1 FE simulation of original design

The original swing arm made from EN-GJS-500 material is calculated to have a mass property of 2.51 kg. FEA on the original design carried out in Ansys show maximum Von Mises stress of 307 MPa located around the edges of the cup. The maximum deformation is small at 0.04 mm, *Figure 21 and Figure 22* displays these results.

Figure 21 - Max Von Mises Stress [MPa] of the original swing arm.

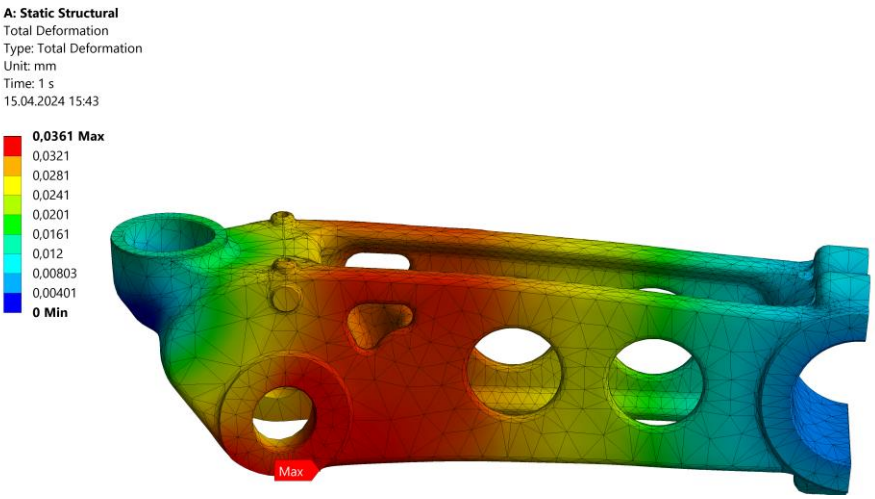

Figure 22 - Max Deformation [mm] of the original swing arm.

5.1.2 Redesign process

In redesigning the swing arm, the initial focus was on identifying a suitable material for our optimized design. The original material for the swing arm, GJS-500, a type of ductile cast iron, was unavailable for 3D printing through any AM techniques found in our research. Therefore, we sought materials with similar ductile characteristics that were compatible with 3D printing. The materials we found to be suitable for our swing arm included Stainless Steel 316L (SS316L) and Titanium Alloy Ti6Al4V. The material and mechanical properties for these alternatives are detailed in

Table 7 [13], [55] *and* [56].

Table 7 - Material properties, optimized swing arm

Properties	Ti6Al4V – Performance	SS316L – Performance	Unit
Density	≥4360	≥7950	kg/m^3
Tensile strength	≥980	≥530	MPa
0.2% Yield Strength	≥900	≥340	MPa
Young's modulus	110	180	GPa
Hardness	≥340	≥200	HV
Poisson's ratio	0.34	0.28	

We began the optimization study by defining the initial geometry, taking into consideration the limitations of the case and preserving the necessary geometric components. We then created a starting geometry that provided the framework for generative design to shape and refine into the new optimized design. The initial geometry for the optimization study is displayed in *Figure 23*.

In this approach, the internal oil channel and fixed components were set as preserved geometry, and the oil channels were framed as piping's within the design. The starting geometry was created as a large block that generative design carved the optimized design from. To ensure that the new optimized design aligns properly with its assembly components, the block was perforated with holes, and some corners were rounded for a more aesthetic result.

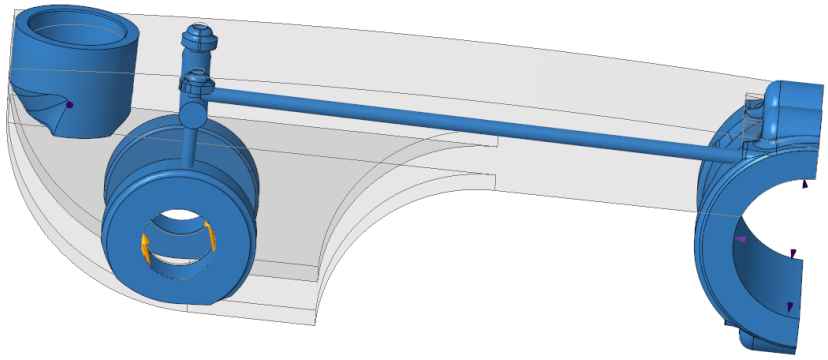

Figure 23 – Generative design initial geometry for the swing arm.

.

The design goal aimed to reduce the starting geometry volume to 40% of its original size. As design criteria, the build direction was set perpendicular to the internal oil channels with a critical angle of 45°. Symmetry was introduced by aligning a symmetry plane along the length of the arm, centered and perpendicular to the build direction. Additionally, a minimum crease radius of 2mm was specified to enhance the design's smoothness.

5.1.3 Optimized design

Multiple iterations exploring various study settings, such as element size, were necessary to successfully convert the generated design into a solid model. This process resulted in a design that features complex geometry and minimal material use, while preserving all essential components. The final redesign of the swing arm is displayed in *Figure 24*.

Figure 24 – Optimized design for the swing arm.

It was important that the redesign did not compromise the functional aspects of the swing arm. Therefore, special attention was given to preserving the internal oil channels, which are essential for the swing arm’s lubrication system. This presented to be a significant challenge, because of the complex nature of the oil channels, these include intricate hollow structures that run through the entirety of the arm. Causing problems for Creo when converting the generated design to a solid model.

As previously mentioned, experimentation was necessary to successfully generate a solid model of the design. At first, models were developed without the oil ducts, resulting in successful solid conversions. Following this, the oil ducts were reintroduced, and several attempts were made using models where the oil ducts were designated as excluded geometry. The result of which was a bulkier design that failed in the transition to a solid model. The reason why this became a major challenge is the problem Creo encounters when trying to generate the reconstructive shapes, which is the conversion of the generated design into solid. The complex geometry necessitated the use of a very fine element size, this cost a lot of computational power, but is necessary to avoid colliding features. The element size is recommended by Creo to be set such that it is smaller than the thickness of small features in the model. A minimum element size of 1.8mm including 109,088 number of elements, resulted in a successful conversion to a solid model with the preserved oil channels, displayed in *Figure 25*.

Figure 25 – Optimized design for the swing arm highlighting preservation of internal oil channels.

Figure 26 displays the final design of the swing arm, complete with its assembly components. The result is an optimized design for AM, which significantly reduces material waste in comparison to its conventional manufacturing method.

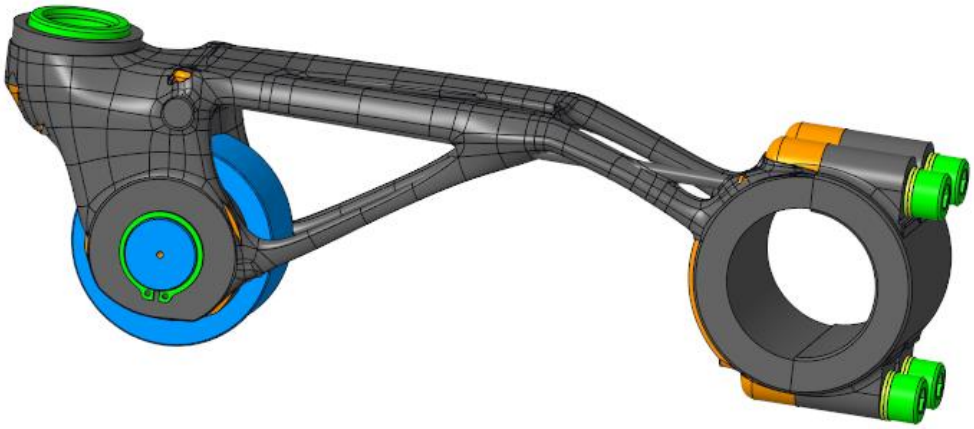

Figure 26 - Final design of the swing arm with assembly components.

FE results

Optimized design SS 316L

The redesigned swing arm, with material specification of SS 316L, achieves a weight of 2.35 kg. This represents a 6% weight reduction compared to the original component. FEA was conducted using Creo's integrated live simulation tool due to meshing issues encountered with Ansys. The analysis revealed that the maximum Von Mises stress occurs in the same region as the original part and is approximately equivalent, measuring at 315 MPa. This stress concentration, identified as a singularity, suggests the stress value is localized to a very small area; thus, the actual stress of this area is likely to be lower. Nevertheless, with a maximum Von Mises stress of 315 MPa, the design remains within the material's 0.2% Yield Strength of 340 MPa, affirming the simulation's accuracy and the redesign's structural strength. The maximum Von Mises Stress for the redesign is displayed in *Figure 27.*

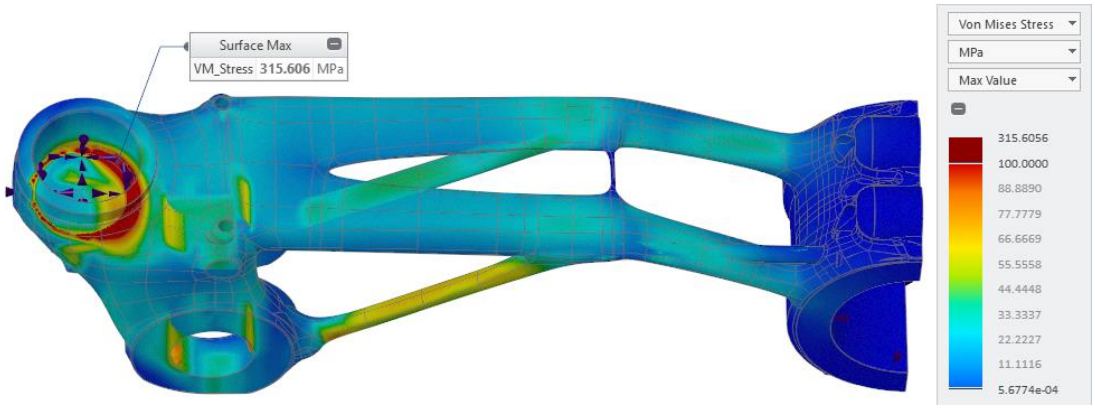

Figure 27 - FEA of the redesigned swing arm in SS 316L, displaying Von Mises Stress [MPa].

FEA performed on the redesigned component indicates a maximum deformation of 0.07 mm, as illustrated in *Figure 28*. This result shows a marginal increase compared to the original part's deformation, yet it is still within a minimal range and localized to the same area as the original design in its original material. Bergen Engines has not defined a critical threshold for deformation, indicating that such a small degree of change is considered negligible and remains within the parameters of acceptable operational deformation.

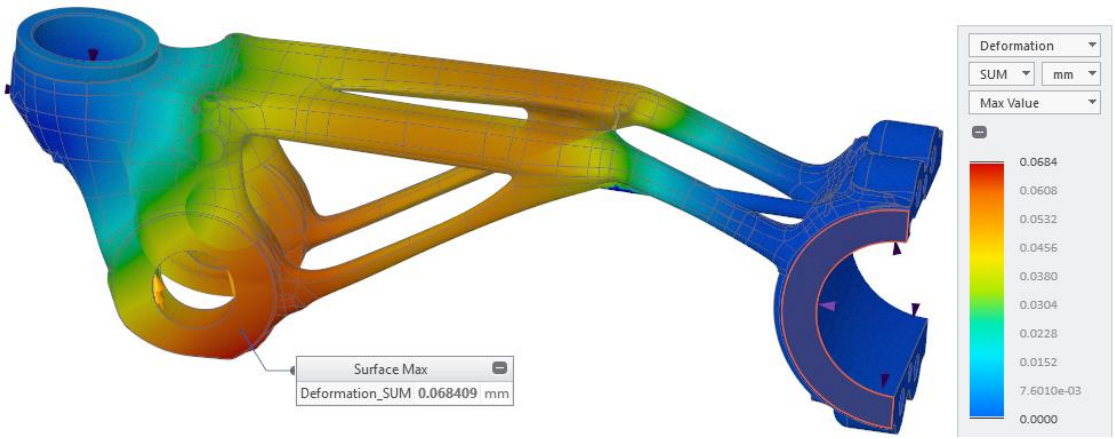

Figure 28 - FEA of the redesigned swing arm in SS 316L, displaying deformation [mm].

Optimized design Ti6Al4V

The design optimized with Ti6Al4V material properties achieves a mass of 1.29 kg, representing a 48% reduction from the original design in its original material. FEA of the Ti6Al4V-optimized design (*Figure*

29) reveals a maximum von Mises stress of 308 MPa, occurring in the same area as the original component. This stress is well within the material's 0.2% yield strength, yielding a safety factor of 2.92.

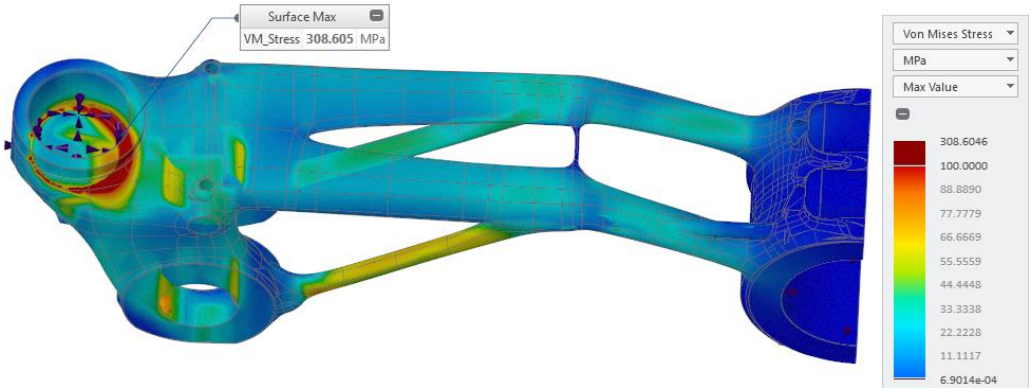

Figure 29 - FEA of the redesigned swing arm in Ti6Al4V, displaying Von Mises Stress [MPa].

Further FEA (*Figure 30*) shows a maximum deformation of 0.11 mm, an increase of 0.07 mm over the original design's maximum deformation. This deformation remains localized to the same area and within the limits of acceptable operational deformation.

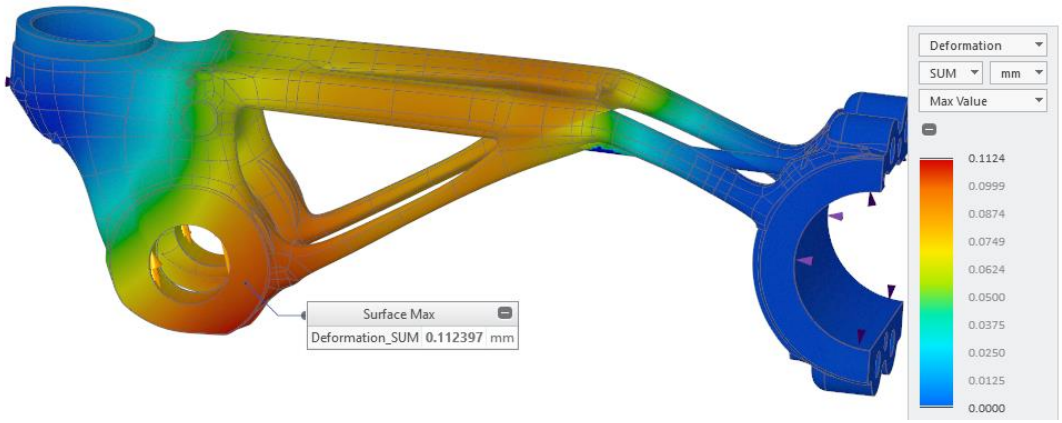

Figure 30 - FEA of the redesigned swing arm in Ti6Al4V, displaying deformation [mm].

5.1.4 Manufacturing process and cost

The original swing arm produced by Bergen Engines is currently priced at 618 €, inclusive of complete assembly, with the machined arm contributing 407 € to the cost. For the optimized design with its material options, the suitable 3D printing technology is PBF, specifically employing SLM or DMLS. These methods ensure the precision and high resolution necessary for the component. The variant made from Ti6Al4V titanium alloy offers a significantly reduced weight but at a substantially higher cost compared to the SS 316L stainless steel version. A cost evaluation, manually estimated by an external manufacturing service, priced the Ti6Al4V version at 9,296 € and the SS 316L version at 4,338 €. These estimates also encompass costs for post-processing treatments and surface finishing [49].

5.2 Case 2 – Spindle

5.2.1 FE simulation original design

To optimize the new design, it is crucial to compare it against the original spindle. A model of the original spindle was created in Creo, and FEA was conducted using ANSYS simulations. This analysis showed that the original spindle experiences a maximum Von Mises stress of 45.7 MPa, and exhibits a deformation of 0.047 mm. These results yield a Factor of Safety (FoS) of 15.5, which serves as a valuable target for the new design. The results are displayed in *Figure 31*.

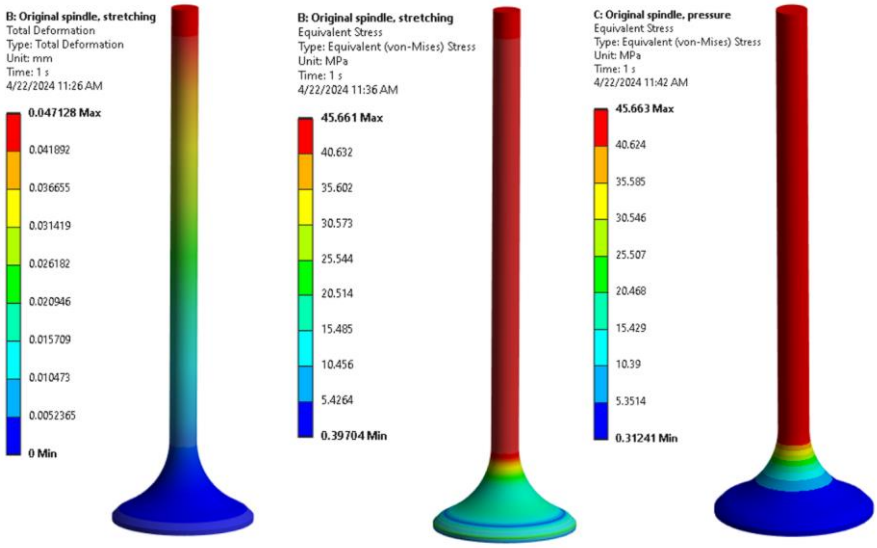

Figure 31 – FEA, original spindle design.

The project started with exploring the original part vs. the shell of the new part. A hollow spindle with the same cross-sectional surface area as the original spindle was created, and simulations were run on the original body as well as the new body. The hollow spindle with the same cross-sectional area, has a wall thickness of 1.17 mm as seen in the Hand Calculations below and *Figure 32*. These tests were done to confirm if the body really needed a wall thickness of 2.00 mm, and to find where the structural problem with the hollow design lied.

Hand Calculations:

$$\boldsymbol{Orginal\ spindle\ design}: \frac{Force}{Area} = \frac{5000N}{(\pi * (6mm)^2)} = 44.2\ MPa$$

$$\boldsymbol{Hollow\ 1.17\ mm}: \frac{Force}{Area} = \frac{5000N}{(\pi * ((6mm)^2 - (2\sqrt{55}mm)^2))} = 44.2\ MPa$$

$$\boldsymbol{Hollow\ 2.00\ mm}: \frac{Force}{Area} = \frac{5000N}{(\pi * ((16mm)^2 - (14mm)^2)} = 26.6\ MPa$$

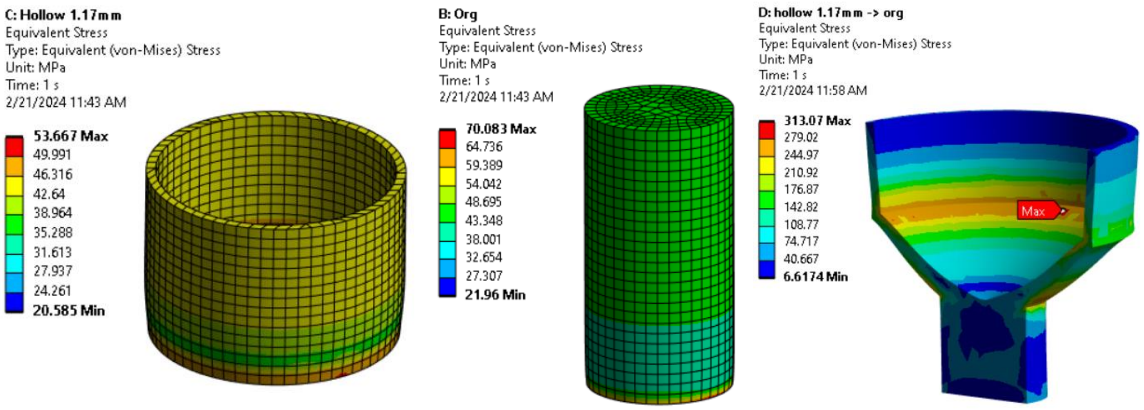

Figure 32 – FEA, 1.17mm thickness hollow body, original body, combination of the two.

We can determine through simulations and manual calculations that using the desired minimum wall thickness of 2.00 mm will result in a reduced maximum von Mises stress compared to the original design. The wall thickness can potentially be reduced to 1.17 mm along the main body. However, retaining a 2.00 mm thickness is preferable since it was requested by Bergen Engines. Also, a 2.00 mm wall thickness would allow for the addition of more layers during the AM process, potentially enhancing the structural strength of the component.

From the simulations shown in *Figure 32*, it is confirmed that the limitations of the new design were not the hollowed body but rather the seam where the diameter of the body changes. From this analysis we can see that our main objective and problem to solve will lie in the transitional area of the part, as marked by the red "Max" probe on *Figure 32.*

5.2.2 Redesign process

On using lattice structure

One solution that was looked at was creating an internal lattice structure for the spindle. This could either work as an internal support or the main structure for structural integrity enhancement. After researching the topic, a gyroid or SC structure were perfered, but due to Creo Parametrics limits on formula driven lattices, it became difficult to simulate a gyroid lattice. To get a starting point to see if this could work, a 2.5D lattice was created as displayed in *Figure 33*.

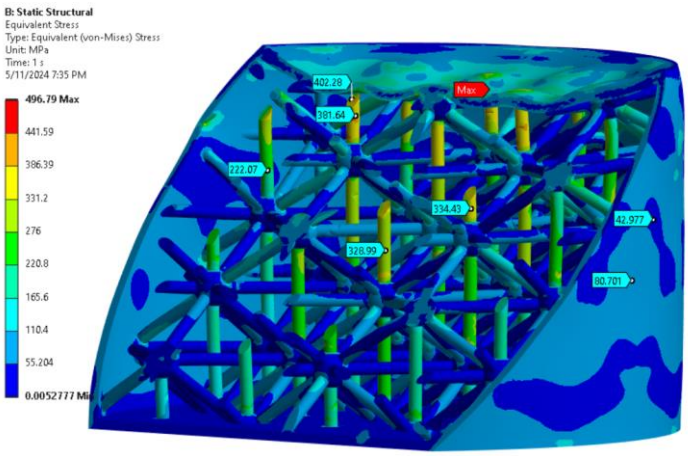

Figure 33 – FEA, 2.5D beam lattice.

The 2.5D beam structure was constructed in Creo and analyzed using ANSYS. This structure was modeled with a body of equal diameter to the spindle, but with a wall thickness of only 0.50 mm. This was done to see the properties of the lattice alone. The simulations estimated the stresses in the lattice to be at max value 496 MPa (Von-Mises's stress), and multiple areas with high values in the 300 MPa range. Although this lattice structure is very different and a lot weaker than a gyroid structure would be, it was found to be insufficiently robust even at maximum density for stainless steel. Consequently, it was determined that this solution would not be pursued further. Instead, the solution requires local reinforcement in the areas discussed in subchapter *5.2.1*, rather than applying reinforcement uniformly across the entire part. Therefore, relying solely on lattice structure alone was not deemed a suitable solution for this case.

Generative design

The redesign of the spindle started with creating a model that could serve as a baseline for the generative design. The Starting geometry and Preserved Geometry were created, and no excluded geometry as the spindle doesn't contain any limitations for the inside. The starting geometry is in line with the designs outer limit, as seen in *Figure 34*, the preserved geometry is blue, while the starting geometry envelops the blue body. The blue body are created with the same measurements, and wall thickness of 2.00 mm, that Bergen Engines required for the redesign of the spindle as seen in *Figure 15*.

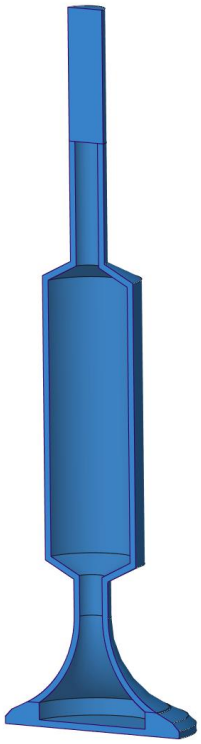

Figure 34 - Staring and Preserved geometry, spindle.

When creating the generative design, we analyzed four distinct scenarios to accommodate two operational states and two material choices. These scenarios included: Titanium grade 5 and Stainless steel C465, each subjected to both compression and tensile loads. *Figure* 35 show how the different loads and supports were affecting the spindle for the generative design.

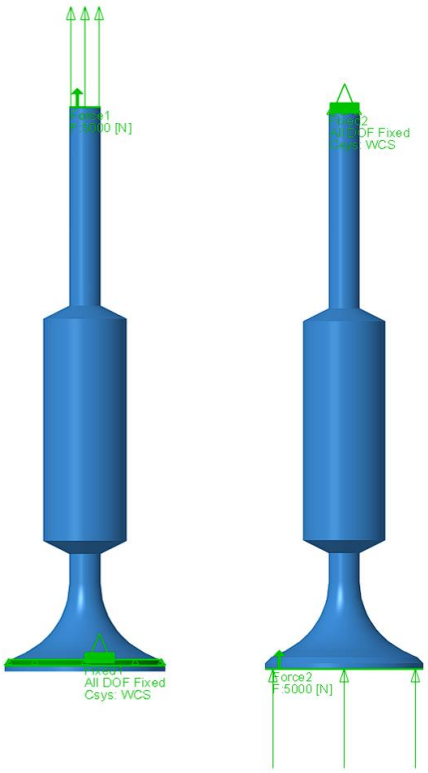

Figure 35 - *Support & Forces applied to the spindle.*

After the creation of the four designs, the designs for compression and tensile loads were measured up against each other. It was recognized that the designs were very similar, and in the case of titanium, they were equal to the naked eye. So, it was decided that the final design for each part would be the compression scenario, since in various iterations in generative design, it was created a structure to support the hollow head of the spindle (*Figure* 36), which the tensile scenario did not include.

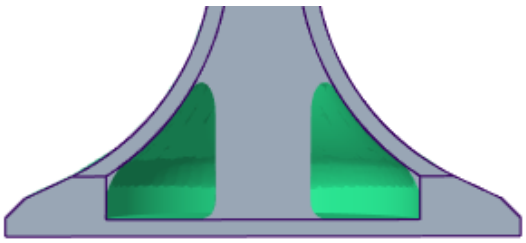

Figure 36 - *Generated rod structure for compression.*

Both the designs were created with a design constraint containing a critical angle of 45° (*Figure 37*). This specification is crucial because the spindle is hollow, and internal support cannot be removed post-production. Therefore, the design was optimized to eliminate the need for any internal support.

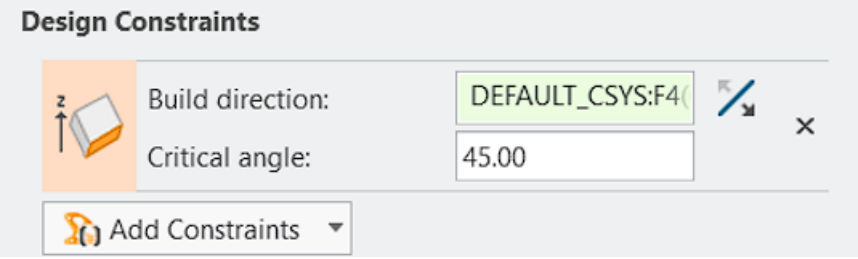

Figure 37 - Critical angle, design criteria in Creo Generative Design.

Material choosing

Choosing the right material is an important part of this task. The material properties in *Table 8* are sourced from Materialise [13], a major company within the AM industry, with access to cutting edge technology. Materialise specifies that all their performance materials, as opposed to their standard materials, can be created with a minimum wall thickness of 0.50mm. Therefore, our design will exclusively utilize these performance materials, as the 0.50mm wall thickness aligns well with our possible need for fine geometries. It is also given that the materials will have a rough surface, which is to be expected, and will require extra steps when producing the part.

Table 8 - Material considerations for Spindle [13]

Properties	**Ti6Al4V - Performance**	**Inconel 625 - Performance**	**SS C465 - Performance**	**SS 316L - Performance**	**Unit**
Density	>4360	>8150	>7840	>7950	kg/m^3
Tensile Strength	>980	>1000	>1600	>530	MPa
0.2% Yield Strength	>900	>760	>1500	>340	MPa
Young - Modulus	110	200	195	180	GPa
Hardness	>340	>300	>550	>200	HV
Poisson's ratio	0.34			0.28	

SS316L has excellent resistance to corrosion in various environments, which is great for our intent of creating a part in contact with gases or fuel. However, it is inferior to the other stainless steel we are considering, the C465, in both strength and hardness. Due to this it is ruled out as a material to consider for the new design.

Inconel 625 is a nickel-based superalloy known for its excellent corrosion resistance, high strength, and good fabricability. Even though it has good strength and hardness properties, it is the densest of all the metals considered, and is not adequate for the design goals of this case.

Titanium grade 5, or Ti6Al4V is a titanium alloy known for its high strength-to-weight ratio and corrosion resistance. Ti6Al4V can be heat-treated to increase its hardness and mechanical properties. These properties, as well as its very low density compared to the rest of the metals, make it an exceptional contender for the final design.

C465 is a strong stainless steel. It has a density close to our original material (see *Table 3*) this makes it easy for us to have a baseline in our design parameters. This stainless steel is also the strongest of the materials under consideration, and it comes out on top with the highest yield strength of all the considered materials. Although this material is denser than the Titanium grade 5, due to its incredible strength and hardness, it will be considered for the final design.

5.2.3 Design 1

Titanium grade 5 design

Given titanium's low density and high strength, the design criteria for this component were established to maintain the original weight of 394 grams while maximizing strength within these constraints. The following design in *Figure 38*, was created with these parameters. The optimized spindle design for Titanium turned out close to a solid, or massive, due to titanium's low density.

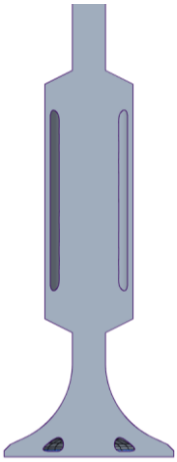

Figure 38 – Optimized design, Titanium spindle.

An argument against this design is its lack of features that are of good value in AM. Since the design is close to massive throughout the spindle, with only very small pockets of air on the sides of the higher diameter section and in the head. One could think of a design with a shorter widened section and make it fully massive and homogenous, as illustrated in *Figure 39*. This could either eliminate AM from the manufacturing process or allow for a faster and less accurate AM method, saving time and cost.

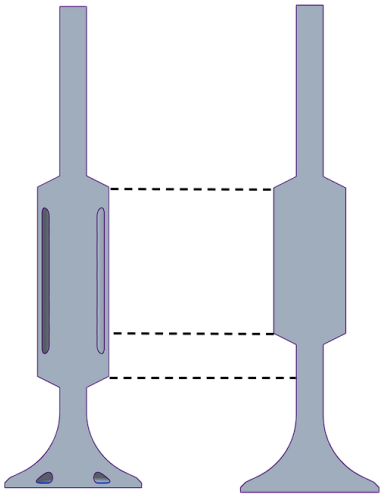

Figure 39 - Titanium spindle alternative design.

FE results

In the design process, FEA revealed a maximum von Mises stress of 55.3 MPa on the part (*Figure 40*). Given the known properties of Titanium grade 5, a Factor of Safety (FoS) of 16.3 was calculated, surpassing that of the original spindle.

With a weight of only 394g, 100% of the original spindle weight, this is a very good result. Looking further at the FEA, we see that it would be possible to create a design with an even lower weight, as the middle section of the spindle barely reaches a Von Mises stress of 15 MPa. However, this could change other aspects of the gas valve and it was chosen to not look at a lower weight solution, even though the titanium design would benefit highly from this.

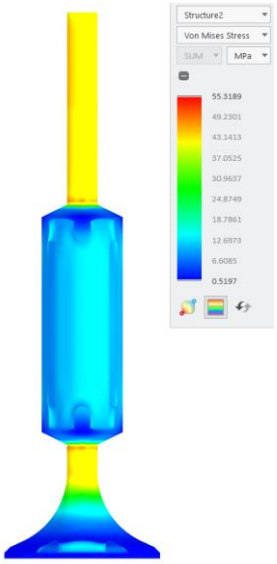

Figure 40 – FEA, Von Mises Stress, Titanium spindle.

The displacement was one of the factors Bergen Engines wanted to minimize. Running a FE alaysis revealed a dissplacement of 0.052 mm. This is close to the original spindle with 0.047 mm displacement and is an acceptable value within our limits. This displacement is displayed in *Figure 41*.

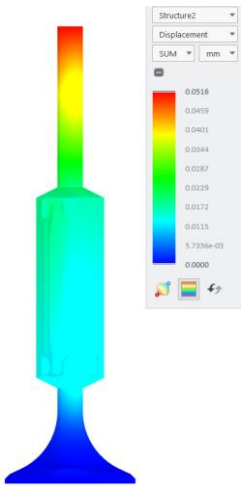

Figure 41 – FEA, max Displacement, Titanium spindle.

An Eigenvalue buckling test was conducted for the top section of the spindle, as it was identified as the most vulnerable to buckling due to its minimal support—being only surrounded by a spring—compared to the more robust, larger diameter section of the body surrounded by the walls of the gas valve. The Eigenvalue buckling test, performed with ANSYS, analyzed 10 buckling scenarios. The weakest force applied for a possible buckling was 7.4 times higher than the expected force of 5kN. This shows us that the design is very strong with a safety factor of 7.4. The analysis had an element count of 26.649, and the total deformation, when 7.4 times the expected force was applied, was 1.144 mm. The buckling simulation is displayed in *Figure 42*.

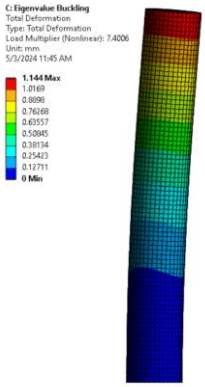

Figure 42 – FEA, Eigenvalue Buckling, Titanium spindle.

5.2.4 Design 2

Stainless steel C465 design

The optimized design for stainless steel was conducted with the same premises as the titanium design, except for weight. Since the stainless steel is a lot denser than the titanium, to match the strength, the weight boundaries were exploited to their fullest, which means as close to 433g as possible. The generated structures within the part, as shown in *Figure 43*, turned out quite as expected from our knowledge of were the hollow body had its weaknesses. This design utilizes the advantages of AM to its fullest. A hollow design with supports in the most critical regions.

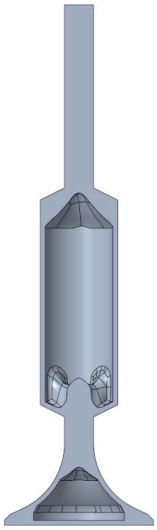

Figure 43 – Optimized design, C465 spindle.

The optimized design had structures within the hollow section of the spindle and filled the smaller diameters part of the body fully. The design was created with the design criteria shown in *Figure 44*. The limit mass seen in *Figure 44* is 412 grams, this is different from the final weight since Creo designs a piece with a higher weight than the limit mass. So even though it is limited to 412g, the total weight turns out to be 432g, which is close to our limit. It can also be seen that some areas of the design are rounded to match the criteria of a 45° critical angle, and our result design could be printed with no internal support structures.

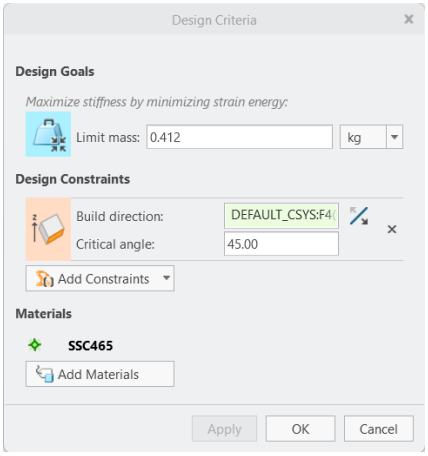

Figure 44 - Design criteria, C465 spindle.

Since the stainless-steel spindle is hollower than the titanium and has smaller features, it was also created a design that allowed for PBF manufacturing, as this method produces product with higher resolution. This design features 2.00 mm holes so that the steel powder has a way to get out of the spindle post manufacturing. These holes have minimal impact on the strength of the spindle, as we will see in the results.

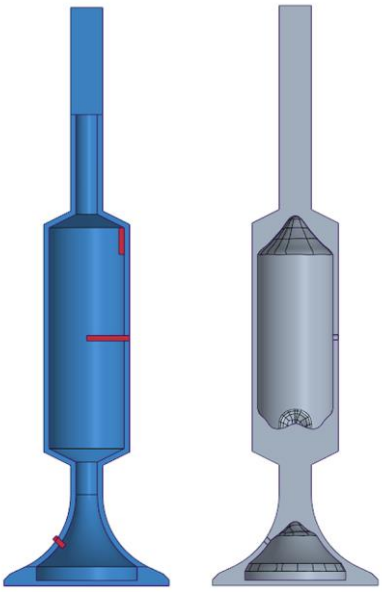

Figure 45 – Optimized design, C465 spindle (powder bed design).

FE results

The optimized design for stainless-steel C465 utilizes the entirety of the 110% weight limit, reaching 432g. The design has a max von Mises stress of 65.0 MPa which points to it strong structural integrity. We can see that the weakest areas are the same as on the titanium spindle, at the base of the lower diameter sections illustrated in *Figure 46*.

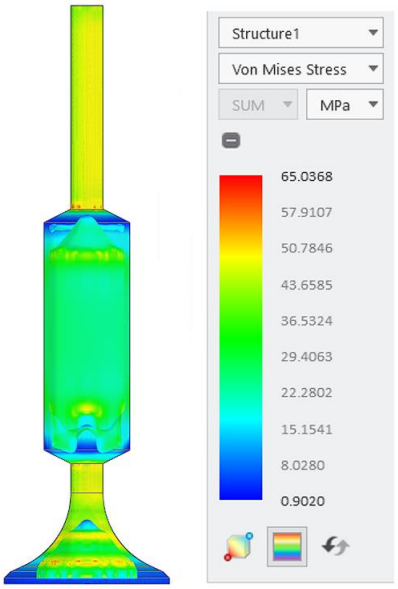

Figure 46 - FEA, Von Mises stress, 1st. C465 spindle.

The same FEA was run on the design allowing PBF manufacturing, with 2.00 mm holes (*Figure 47*). With a stress value of 64.7 MPa it is as strong as the part without holes. This confirms that this design would not have any specific structural weaknesses due to its features, and a powder bed manufacturing method would be possible. Both designs have a calculated Safety Factor of 23.

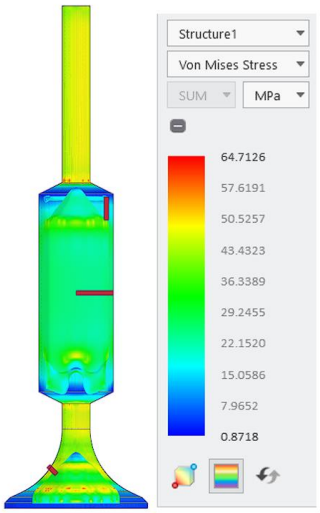

Figure 47 – FEA, Von Mises stress, 2nd. C465 spindle

The FEA reveals a total displacement of 0.065mm for the stainless-steel design. This is a little higher than what we would want, but it is still within our boundaries. As we can see from *Figure 48*, the weakest spot is at the end of the spindle head. The displacement should not be an issue, but it could be reduced by introducing a small rod internally in the head like seen in *Figure* 36.

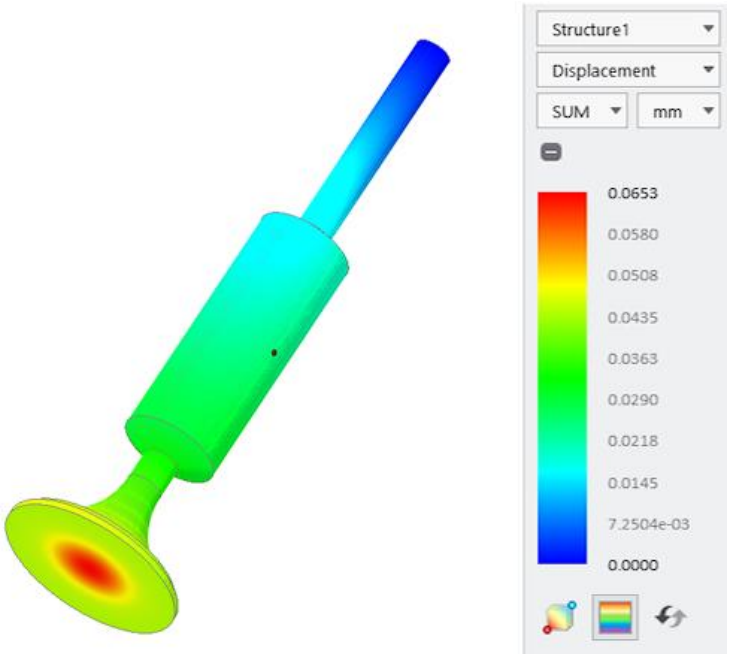

Figure 48 – FEA, max Displacement, C465 spindle.

The Eigenvalue buckling for the stainless steel (*Figure 49*) was done on the same premises as the titanium. It was shown that the stainless steel was even stronger than the titanium, which was expected due to its superior strength properties. With a Safety Factor of 15.3 it shows great structural integrity.

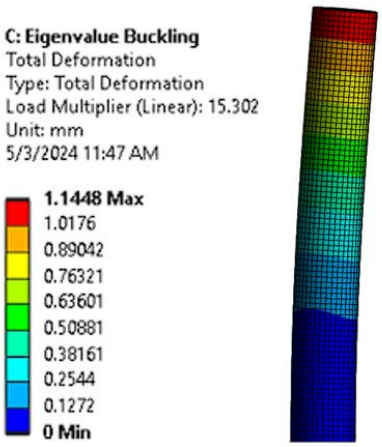

Figure 49 - Eigenvalue buckling, C465 spindle.

5.2.5 Manufacturing process and cost

Titanium spindle:

The best solution for the titanium spindle would be to use Norsk Titanium's Rapid Plasma Deposition method. This method would create a strong homogenous spindle, with stronger properties than other methods would provide. Since the spindle would be massive, the bigger layer thickness and height that this method provides would not be any hinderance, and only improve the creation time and cost. After the printing process the part would have to be surface finished on a lathe.

C465 spindle:

Manufacturing recommendations for the C465 spindle would be Selective Laser Melting. As a powder bed method, this offers superior accuracy and higher resolution than Direct Laser Deposition methods. Out of the powder bed methods we have discussed and researched, the SLM method is the one that produces the strongest product and would be the best way to produce this part.

After the printing process the powder would have to be removed from the spindle. After the powder is removed the holes can be welded if needed. This would prevent any possibility of oil or lubricant entering the spindle and filling it over time.

It's important that the spindle has a smooth surface finish for movement with minimal friction in the gas valve. After welding it shut, it would have to be put on a lathe to achieve this finish, it is also important to consider layer cavities as explained in subchapter *2.1 Manufacturing technology*.

Price estimation:

Price estimations for the different spindle designs manufactured with SLM gives a price of 2,500 € for the Titanium spindle, and 2,000 € for a SS316L spindle (*Figure 50*). The reference for price estimation did not have C465 steel available, so 316L stainless steel was used to receive an estimation. However, the estimations still highlight the difference in material cost from steel to titanium.

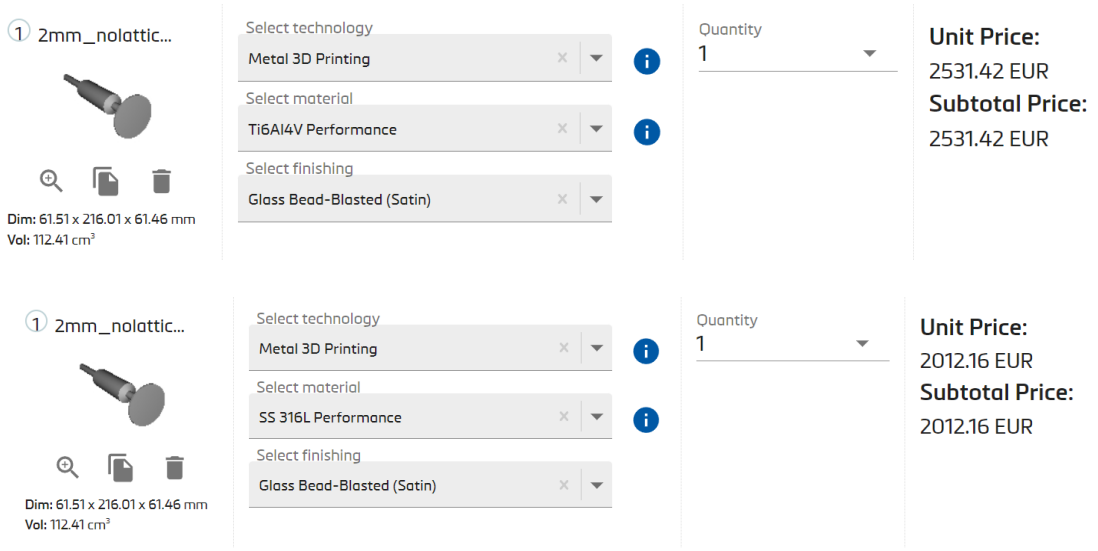

Figure 50 - Spindle 1st. price quotation.

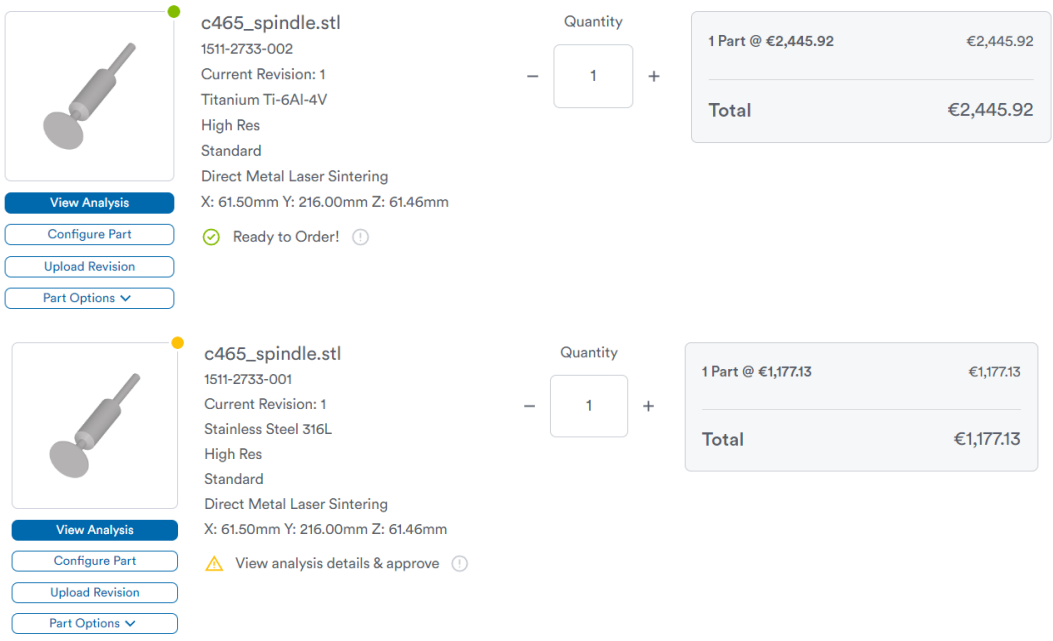

Figure 51 - Spindle 2nd. price quotation.

A second price estimation from another reference gave us a quotation of 1,177 € for the same SS316L spindle using the same manufacturing process, while the titanium spindle remained at the same price (*Figure 51*). This shows us the market for outsourcing manufacturing of these parts have very varied price points.

This price estimation is without the proper surface finish that the part requires, and only one part. To get the required surface finish the parts need to be polished on a lathe, which would add to the cost. At the same time, creating more than one part would decrease the cost per part.

5.3 Case 3 – Camshaft extender

The redesign of the camshaft extender aimed to optimize the components for AM by simplifying the assembly and reducing weight. The design also needed to meet specific criteria, including the fatigue limit and material yield strength. This process proved challenging, requiring multiple design modifications.

5.3.1 FE simulation original design

To evaluate the effectiveness of our redesign, FEA was initially conducted on the original components of the camshaft extender. This analysis is beneficial for validating the performance of our redesigned components. It helps us to determine the reliability of the results, assess potential design failure, and verify any improvements in structural strength. The FEA revealed a maximum deformation of 0.18 mm for the original camshaft connection and 0.09 mm for the mount connection. Although Bergen Engines has not specified a maximum allowable deformation, comparing these values with those from our redesign remains a point of interest. The FEA results showing the deformation of the original parts are displayed in *Figure 52*.

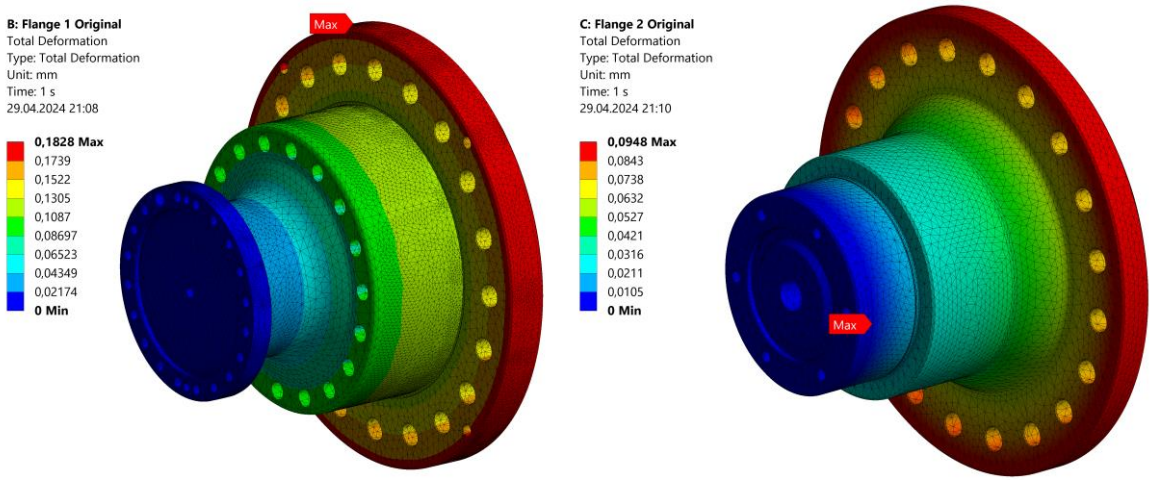

Figure 52 – FEA, total deformation, original camshaft extender.

Figure 53 illustrates the equivalent Von Mises stress for both components. The results indicate that the stress values for both components are significantly below the yield criterion of their material, 42CrMo4, which has a yield strength of 500 MPa. This suggests that the components are overengineered, containing excessive material and contributing to unnecessary weight. This observation provides a basis for considering material reduction in future redesigns without compromising the structural integrity of the components.

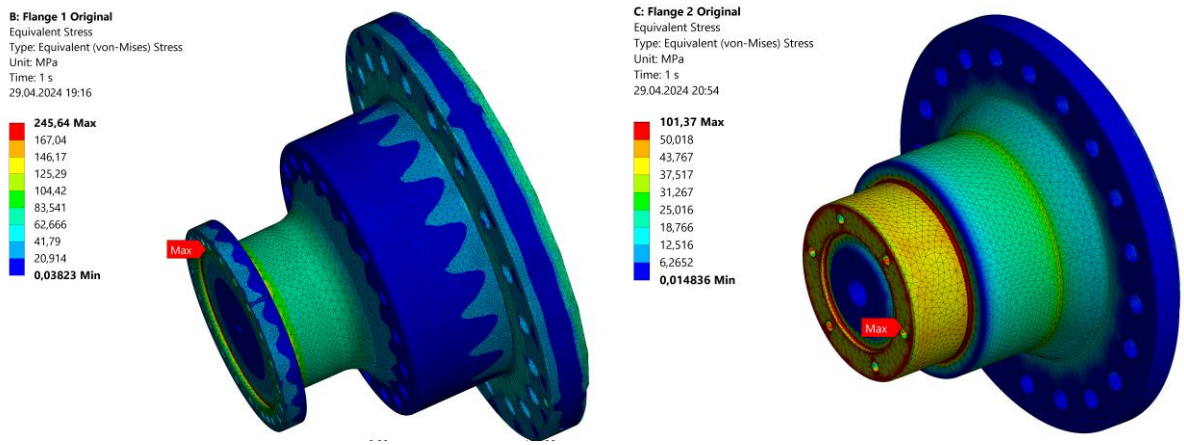

Figure 53 - FEA, Equivalent Von Mises stress, original camshaft extender.

When evaluating the fatigue limit of 250 MPa, it is essential to consider both the maximum and minimum principal stresses. In Ansys, the highest actual principal stress derived from the analysis may not always be displayed in the maximum principal stress results; it can sometimes appear in the minimum principal stress data. For the original components, the highest principal stress value was recorded as the minimum principal stress. The FEA results indicated a maximum principal stress for the camshaft connection at 251 MPa, just above the fatigue limit, and for the mount connection, a stress of 144 MPa, which is comfortably below the fatigue limit. However, it's important to note that simulations may present artificially high values, suggesting that the actual stresses experienced by the components could be lower. The result for prinicipal stress is displayed in *Figure 54*.

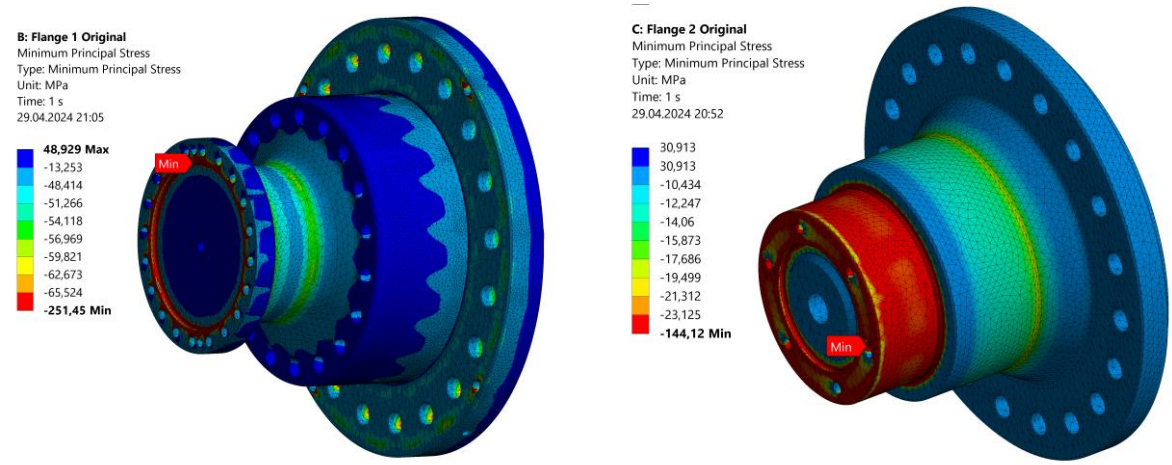

Figure 54 – FEA, maximum principal stress on the original camshaft extender.

The original components of the camshaft extender have substantial mass, with the camshaft connection weighing 102.64 kg and the mount connection at 82.68 kg, resulting in a combined weight of 185.32 kg. This substantial weight can present challenges when installed in the confined spaces of the engine block. Moreover, this total weight does not consider the additional mass of other assembly components such as the gearwheel, which further complicates installation in tight spaces. These factors highlight the advantages of reducing component weight in our redesign, potentially easing installation and enhancing the overall efficiency of the assembly process.

5.3.2 Redesign process

To optimize the design of the camshaft extender, we aimed to reduce both the number of assembly components and the overall weight. This redesign leveraged Creo's generative design capabilities, an approach well-suited for the relatively simple geometry of the two bodies involved. The redesign's main objective was to decrease the number of components from four to three by integrating the camshaft connector with its associated flange (illustrated in *Figure 55*).

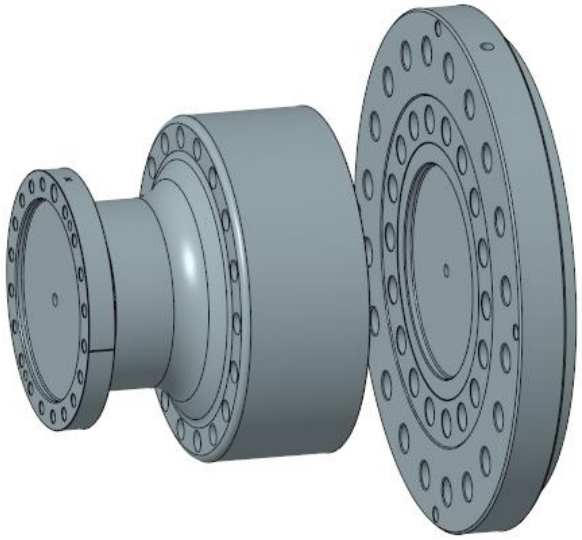

Figure 55 - Camshaft connector with is associated flange.

The gearwheel was maintained unchanged to preserve its dimensions and ensure its adjustability with the camshaft connection. This requirement necessitated keeping a two-part division in the axle at the location of the gearwheel. Consequently, the redesign focused on the extender for the camshaft and the mounting flange, redesigning each part separately.

Our initial step in the generative design process involved defining the study parameters, including preserved and starting geometries. To facilitate optimization, manual modifications were applied to simplify the preserved geometries. The two broad flanges connecting to the gearwheel were extruded and simplified, excluding chamfers and threads for the bolt connections. In the final design, these flanges were replaced with its original flange and merged with the reconstructed geometry. The starting geometry was designed as a large cylinder encapsulated within the preserved geometries. The generative design studies for the camshaft connection and the mount connection are displayed in *Figure 56* and *Figure 57*.

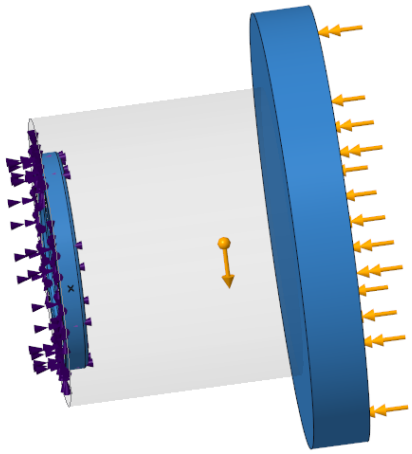

Figure 56 - Generative design study for the camshaft connection.

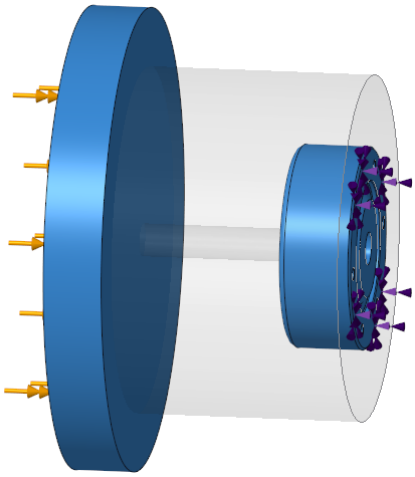

Figure 57 - Generative design study for the mount connection.

Subsequent steps included defining the necessary loading and boundary conditions for the design study, adhering to the specifications outlined in the case definition. Standard earth gravity conditions were applied to both design studies. The material selected was 42CrMo4, chosen for its compatibility with 3D printing technologies and used in the original part. The design goal was set to “optimize stiffness’ to minimize material waste and reduce weight. Finally, the design criteria established to guide the redesign included 'build direction' with a critical angle of 45 degrees, and 'rotational symmetry' with the symmetry axis centered along the part's midline.

In the process of achieving a final redesign for the camshaft extender, multiple redesigns were necessary to meet the design and safety criteria specified in the case definition. Initially, we were pleased with the design's aesthetics; however, simulation results revealed maximum principal stresses that exceeded the fatigue limit of 250 MPa. To achieve a final design that meets all design criteria, multiple redesign efforts were undertaken. Each iteration varied in design goals, study settings, and manual adjustments.

5.3.3 Design 1

The initial redesign for the camshaft connection was set with a design goal of reducing its volume to 27% of the original. The study utilized a minimum element size of 4.65 mm, determined by a fidelity setting of 6, which resulted in 159 372 elements. This fine element setting was necessary because attempts with smaller elements failed during the geometry reconstruction process. The results from this first redesign of the camshaft connection are displayed in *Figure 58*.

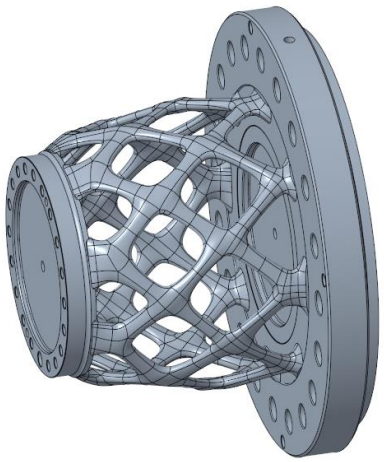

Figure 58 - First redesign for the camshaft connection.

For the mount connection, which started with a lower volume than the camshaft connection, it was necessary to preserve a higher percentage of material to achieve a pleasing design. The design goal was set to reduce the volume of the starting geometry to 35% of the original. This required several trials with varying percentages of preserved material to reach an acceptable outcome. The study settings here included an element size of 4.90 mm, again determined by a fidelity setting of 6, resulting in 159,371 elements—a similarly fine element size. This was necessary for successful geometry reconstruction. The results of the first redesign for the mount connection are displayed in *Figure 59*.

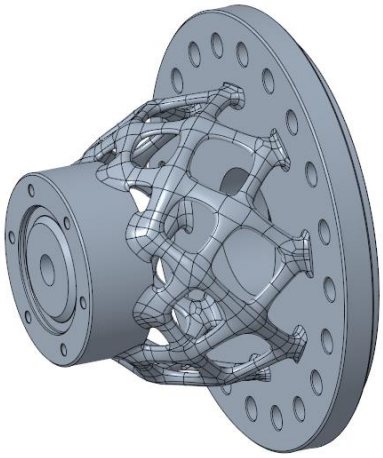

Figure 59 - First redesign for the mount connection.

After redesigning the two parts, they were integrated into the original assembly file to evaluate their compatibility with the existing assembly components. As illustrated in *Figure 60*, the complete setup with the optimized flanges is shown to be fully compatible with both the gearwheel and the bolted connections. By merging the cam ring with its corresponding flange, as mentioned earlier, we successfully eliminated the need for a separate bolted connection between them. This integration not only reduces assembly time but also minimizes the number of bolts required.

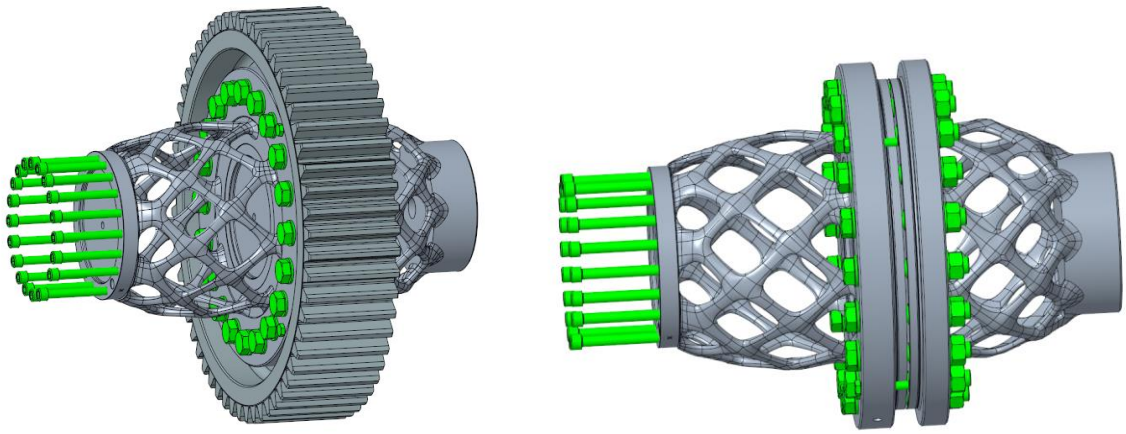

Figure 60 - Assembly of the first redesign camshaft extender.

FE results

The first redesign resulted in respective weights of 52.51 kg for the camshaft connection and 54.96 kg for the mount connection, reflecting a shift in the weight ratio between the two components. Together, they total 107.47 kg, marking a 42% reduction from the original combined weight.

FEA analysis of the redesign revealed a maximum total deformation of 0.45 mm for the camshaft connection and 0.34 mm for the mount connection. Although these values represent an increase from the original components, the deformations are still minimal. The deformations are illustrated in *Figure 61*.

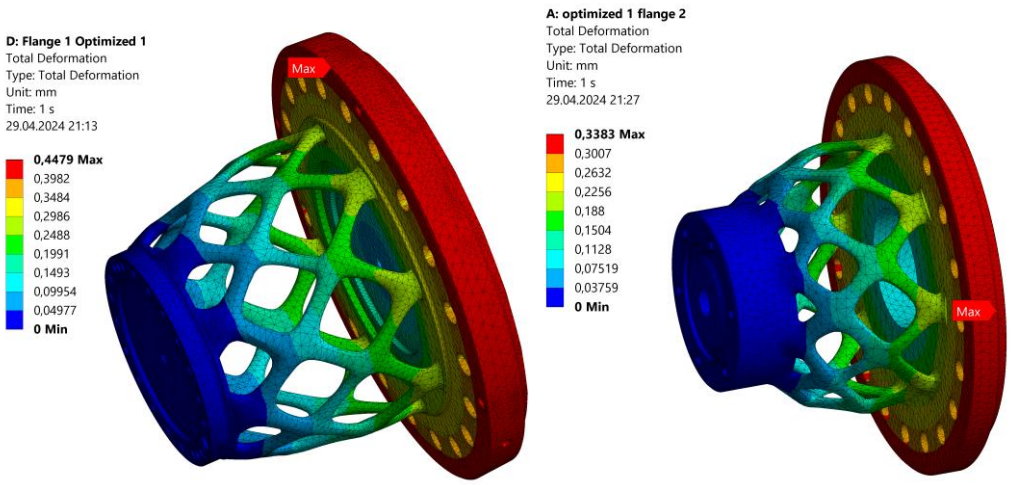

Figure 61 – FEA, Total Deformation, Design 1.

Subsequent analysis showed a significant increase in the Von Mises stress for both components compared to the original design. These values remain well below the material's yield strength of 500 MPa but suggest that our maximum principal stress exceeds the fatigue limit of 250 MPa. These results are presented in *Figure 62*.

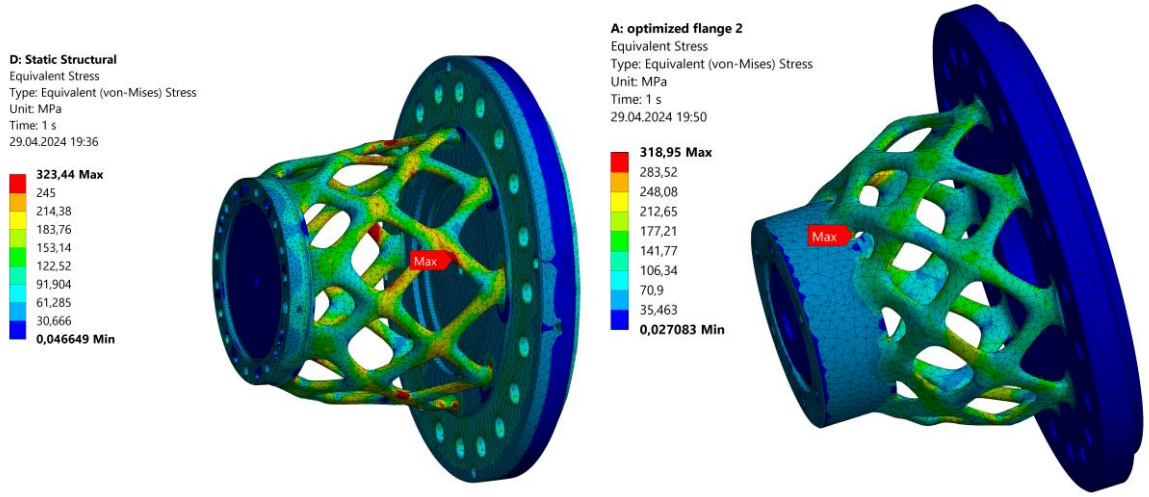

Figure 62 – FEA, equivalent Von Mises stress, Design 1.

FEA indicated a maximum principal stress of 354 MPa for the camshaft connection (*Figure 63*), a value which might be categorized as a singularity. Singularities, common in FE simulations, manifest as artificially high stresses concentrated in single elements or very small areas. Despite this, larger regions displaying high stress concentrations were also observed, with stresses around 280 MPa—exceeding the 250 MPa fatigue limit. These findings are displayed in *Figure 64*.

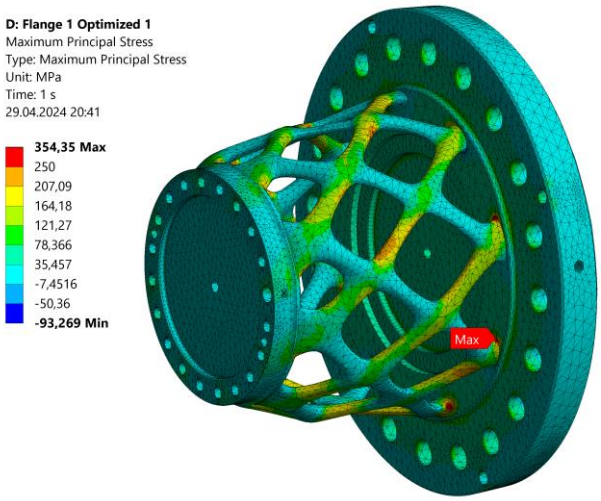

Figure 63 - FEA, Principal stress, camshaft connection.

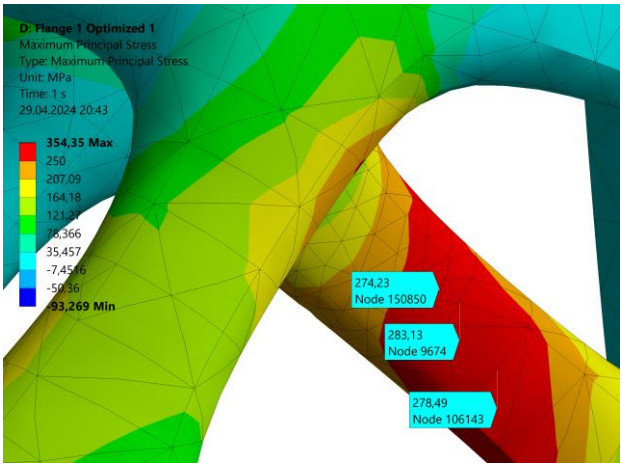

Figure 64 – FEA, high stress concentrations, camshaft extension.

Similarly, for the mount connection, principal stresses significantly above the fatigue limit of 250 MPa were detected, as depicted in *Figure 65*. These elevated stress levels necessitated further review of our design to identify potential modifications that could reduce these stresses.

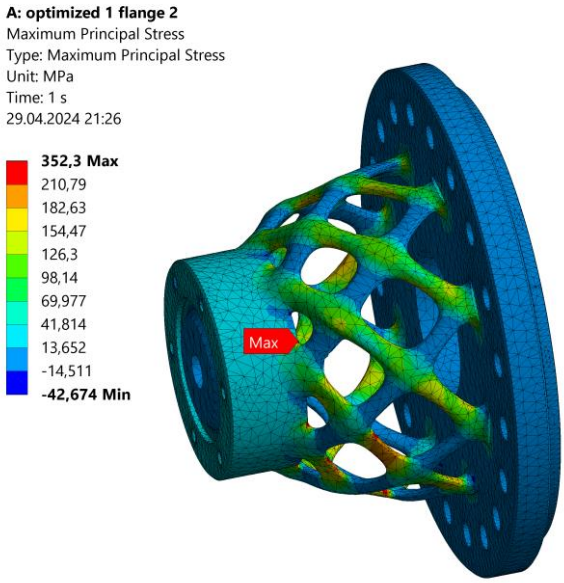

Figure 65 – FEA. Principal stress, mount connection.

5.3.4 Design 2

To align our design with the specified fatigue limit of 250 MPa, we sought to manually refine transitions within the design. The geometric characteristics of a component can significantly influence its fatigue properties. Notches and discontinuities act as stress raisers and potential sites for fatigue crack initiation. The sharper the discontinuity, the greater the stress concentration, thereby increasing the likelihood of fatigue failure. To mitigate this risk, our approach involved eliminating sharp corners and sudden contour changes through design modifications [57].

As part of these modifications, rounded corners were introduced to the preserved geometry, as illustrated in *Figure 66*. These enhancements were made prior to initiating the optimization study, with the design

goals and settings remaining consistent with those of Design 1. Post-optimization, a plateau was added to the widest section of the flange, and the corners were further rounded to smooth the transition between the flange and the mount. This new plateau is displayed in *Figure 67*.

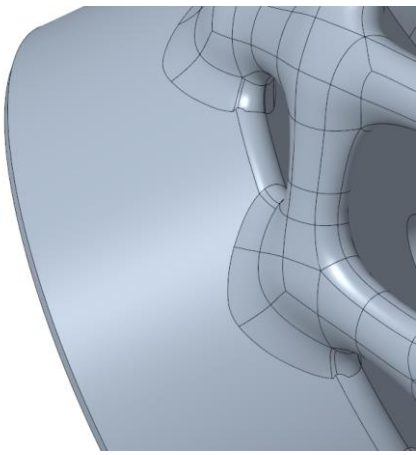

Figure 66 - Rounded corners of the preserved geometry, design 2, camshaft extender.

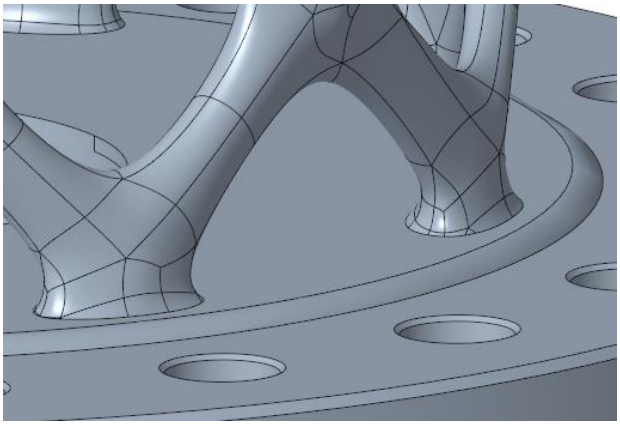

Figure 67 - Plateau for smoother transitions, design 2, camshaft extender.

Figure 68: Complete Design 2, showcasing the modifications aimed at enhancing the component's fatigue resistance. This revised design was implemented initially to evaluate the effectiveness of the changes. Depending on the results, similar modifications might be considered for the camshaft connection, or further adjustments to the optimization study parameters, such as preserved mass, might be necessary.

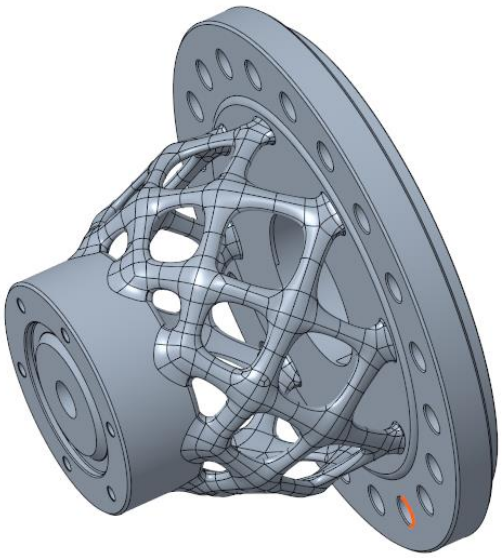

Figure 68 - Complete Design 2, camshaft extender.

FE results

FEA of the second design illustrates the positive effect of smoother transitions on reducing stress concentrations. The maximum Von Mises stress was reduced to 277 MPa, while the maximum principal stress was reduced to 305 MPa. Although the maximum principal stress still exceeds the fatigue limit of 250 MPa, these outcomes provide valuable insights for subsequent design modifications. The simulation results for Design 2 are displayed in *Figure 69*, highlighting these improvements.

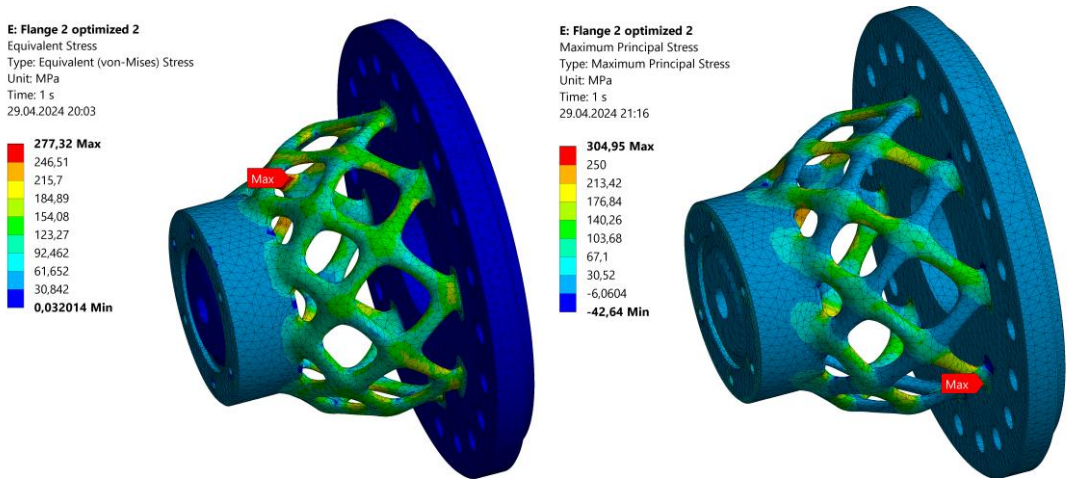

Figure 69 – FEA, Design 2, camshaft extender.

5.3.5 Design 3

In response to previous findings, it was decided to combine smoother transitions with an increased percentage of preserved volume for the optimization study. For the camshaft connection, a new study increased the preserved volume to 30%, up from 27% in the initial design. This study used a minimum element size of 4.15 mm, dictated by a fidelity setting of 7, resulting in 223,140 elements that successfully reconstructed the geometry for Design 3. This resulted in a slightly heavier design with more preserved mass aiming to improve structural strength. Design 3 for the camshaft connection is displayed in *Figure 70*.

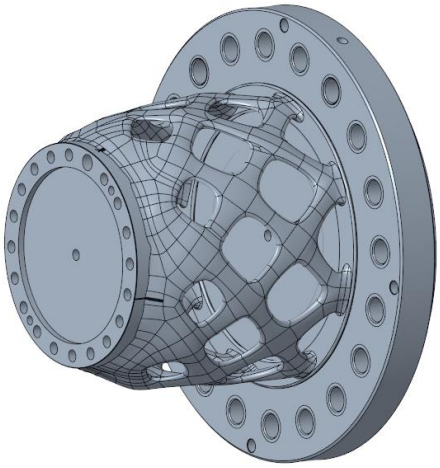

Figure 70 - Design 3 for the camshaft connection.

For the mount connection, modifications to the starting geometry were made to achieve a pleasing design. These modifications involved increasing the diameter of the starting geometry, resulting in a slightly higher volume. A design goal was set to reduce the volume to 32% of the original, which, although lower than the previous optimization study, allowed for a greater retained volume due to the increased diameter. The design required precise optimization settings, with a minimum element size of 3.96 mm and a fidelity level of 8, resulting in 301,937 elements that successfully reconstructed the geometry. This resulted in a design that is slightly heavier than previous versions but aims to improve structural strength. Design 3 for the mount connection is displayed in *Figure 71*.

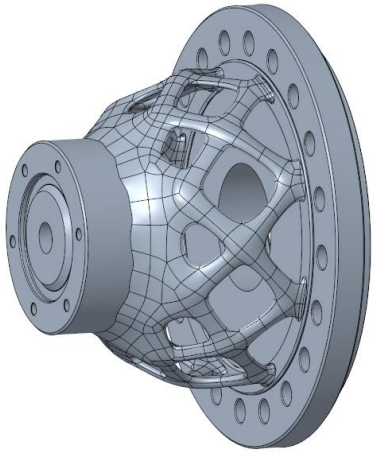

Figure 71 - Design 3 for the mount connection, camshaft extender.

Figure 72 displays the assembly of the complete camshaft connection with Design 3, illustrating its compatibility with the gearwheel and bolt connections. The increased diameter at the mount connection reduces the available space for the M20 bolts that connect the two parts. While the assembly file indicates that the bolts fit adequately, the limited space could complicate the assembly of the gearwheel. This issue will require further evaluation in a prototype setting.

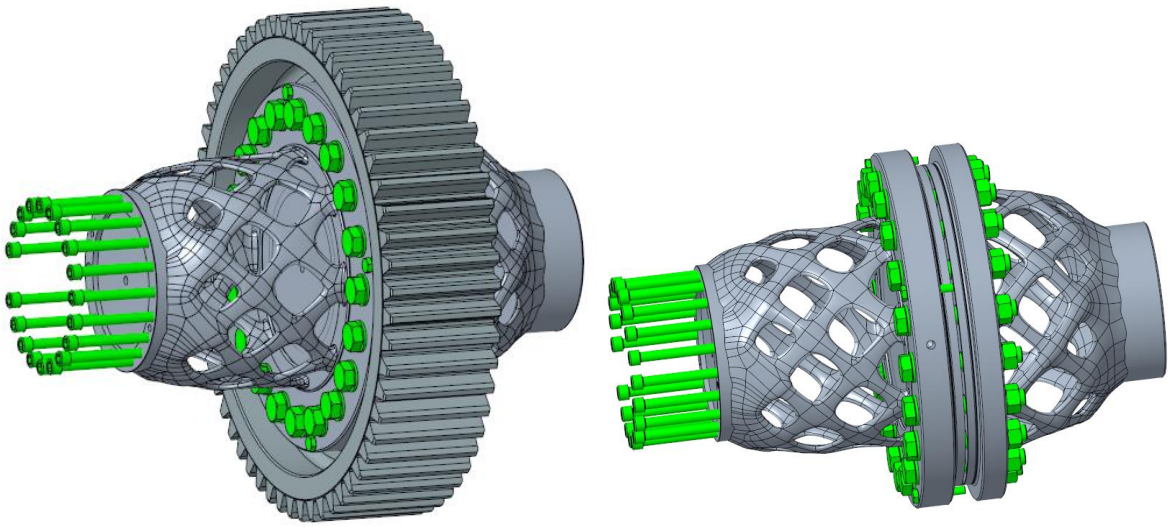

Figure 72 - Assembly of design 3 camshaft extender.

FE Results

FEA of Design 3's two components revealed a maximum deformation of 0.35 mm for the camshaft connection, showing only a minor increase from the original part. The mount connection exhibited a maximum deformation of 0.24 mm, an increase of 0.15 mm from its original, yet still representing a minimal deformation. The deformation under load for both components is depicted in *Figure 73*.

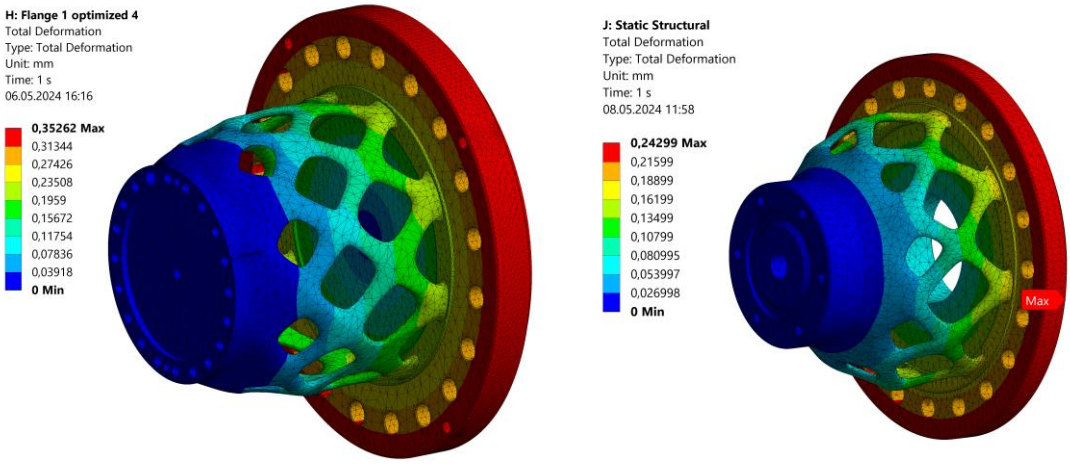

Figure 73 – FEA, Total Deformation, Design 3, camshaft extender.

The FEA results indicated a maximum Von Mises stress of 252 MPa for the camshaft connection, closely mirroring the original part and remaining well below the material's specified yield strength. For the mount connection, a maximum Von Mises stress of 206 MPa was observed, an increase from the original but still within acceptable limits. The equivalent Von Mises stress for both components are illustrated in *Figure 74*.

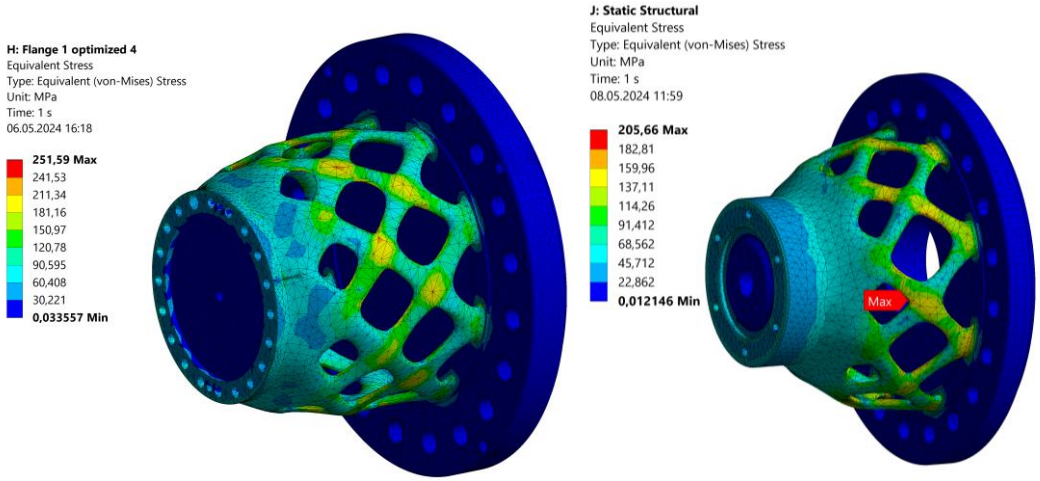

Figure 74 – FEA, Equivalent Von Mises stress, Design 3, camshaft extender.

Principal stress, which was a major issue in previous designs, has been addressed in Design 3 through smoother transitions and a higher percentage of material preservation. These modifications have helped keep the stress values within the specified fatigue limits. Specifically, the maximum principal stress recorded was 248 MPa for the camshaft connection and 219 MPa for the mount connection, both of which satisfy our design criteria. It should be noted, however, that these values may be somewhat higher than actual real-world values due to the nature of simulation. The principal stress for both components is depicted in *Figure 75*.

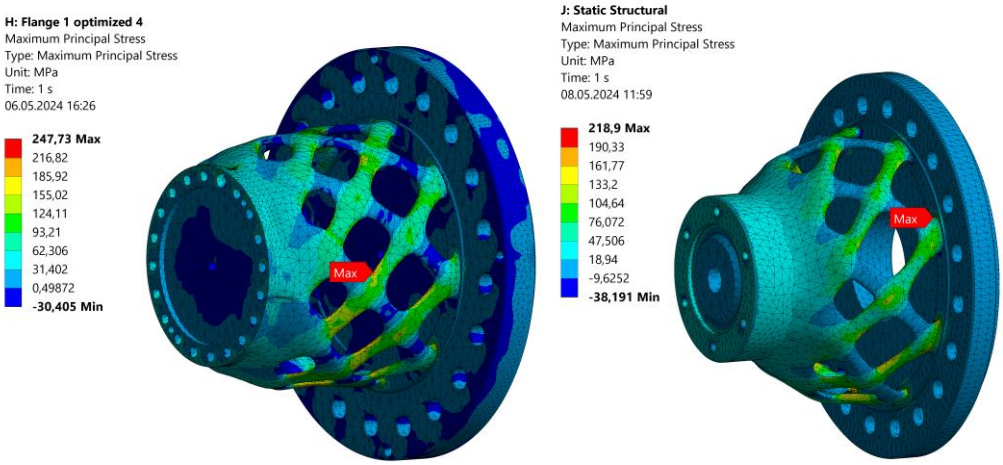

Figure 75 – FEA, Principal stress, Design 3, camshaft extender.

The mass of the camshaft connection is calculated at 53.30 kg and 57.00 kg for the mount connection, indicating a shift in the weight ratio between the two components compared to the original. Together, the components weigh 110.3 kg, marking a slight increase from the first design but still achieving a 40% reduction in weight from the original components.

5.3.6 Manufacturing process and cost

The original mount connection has a production cost of 1,547 € in its original material, and the mount connection a production cost of 1,479 €. Both the optimized components would be manufactured using the same material, specifically 42CrMo4. The most suitable printing technology for this is PBF, specifically through SLM. Due to the large dimensions of the components, a larger printer is necessary.

We contacted manufacturers for cost estimates, but unfortunately, all the manufacturers we reached out to have a limited build size of 280 × 280 × 350mm in the X, Y, and Z directions respectively. The camshaft connection measures 415 × 415 × 274mm, and the mount connection measures 415 × 415 × 257mm. Therefore, we were unable to receive a cost estimation for the parts from these manufacturers. However, we did receive an estimate for the material at 6-10 €/cm^3. The total volume of the camshaft connection is 6,829cm^3, with a conservative estimation of 10 €/cm^3, resulting in a material cost equivalent to 68,290€. For the mount connection, with a total volume of 7,309cm^3, the material cost is calculated to be 73,090 €.

The gearwheel, which was not further redesigned for AM from the original design, could also be printed using PBF trough SLM. A suitable material for this component would be EOS Case Hardening steel 20MnCr5, which is eligible for 3D printing and has similar properties to the original material 18CrNiMo7-6. This part would also require a larger 3D printer as the part measures at 570 × 570 × 136mm. Typical properties for 20MnCr5 are noted in *Table 9* [58], [59] .

Table 9 – Typical component properties for 20MnCr5 [60] *and* [61]

Properties	20MnCr5	Unit
Density	7800	kg/m^3
Tensile strength	≥1250	MPa
0.2% Yield strength	≥900	MPa
Young – modulus	210	GPa
Hardness	≥60	HRC
Poisson's ratio	0.3	

5.4 Case 4 – Wheel for probing

5.4.1 Redesign process

Looking at the specifications for the probe wheel (*Table 6*), density and thermal expansion are two extremely important properties for this tool. Titanium, known for its high strength to weight ratio, offers a stiffness close to that of steel, making it a good alternative. Titanium's thermal expansion coefficient ranges from 8.7 to 9.1 [62] which is lower than 42CrMo4's coefficient of 11.1 [63]. The Titanium also has a way lower density compared to the previous material which will help a lot in weight reduction. Creating the part out of Ti6Al4V would be optimal for this tool.

Table 10 – New [13] *and old* [19] *materials, wheel for probing.*

Parameters	Ti6Al4V – Performance	42CrMo4	Unit
Density	≥4390	7800	kg/m^3
Tensile Strength	≥980	700-1230	MPa
Yield Strength	≥900	500	MPa
Young – modulus	110	210	GPa
Hardness	≥340		HV
Poisson's ratio	0.34	0.3	
Thermal Coefficient	8.7 – 9.1	11.1	$10^{-6}/K$

After deciding what material fits best for our task, the redesign of the wheel for probing continued with importing the geometry given to us by Bergen Engines into Creo. The Original geometry served well as a template for marking out the important features, as well as finding its volume and weight. Around this model, some new bodies were created. The Starting geometry (

Figure 76), the preserved geometry in blue (*Figure 77*) and the excluded geometry which can be seen in red (*Figure 77*).

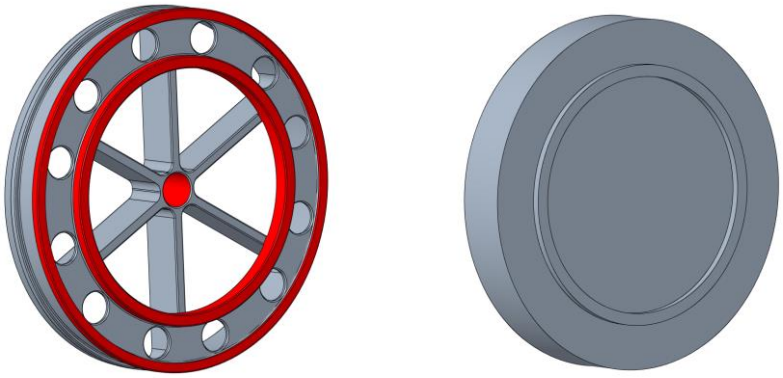

Figure 76 – Creo Generative, Original design & Staring geometry for Wheel.

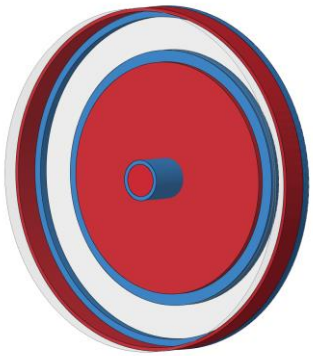

Figure 77 – Creo Generative, Preserved & Excluded geometry for Wheel.

When creating constraints for the optimization the middle cylinder was put on a fixed cylindrical support, which means it can rotate like it would on a lathe. This support is marked with a dark purple color (*Figure 78*).

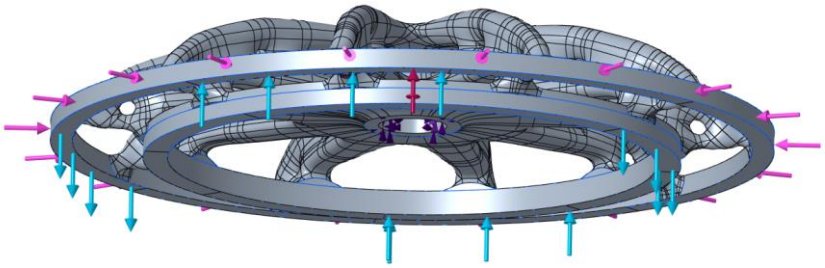

Figure 78- Creo Generative, Forces applied for the redesign of the probe wheel.

Taking some tips from a machining specialist [64] we find that a good turning speed for titanium is 150 surface feet per minute (SFPM). Doing the calculations for converting this to RPM, we find that this equals 45.15 RPM for our wheel. This is not that fast but was still taken into consideration when creating the design criteria. This is included as a design criterion as a Centripetal force market with the red arrow (*Figure 78*). This is important so that the wheel can stay stable during the machining process, and we get a final product that is concentric and accurate.

The Blue arrows are simulation of forces, there are forces of 1kN spread over an area of ¼ π. There are four sones, two on the outer ring and two on the inner, each going in a direction up or down. These are there to represent bending or other types of abuse that a measuring tool typically can go through in a workshop type environment.

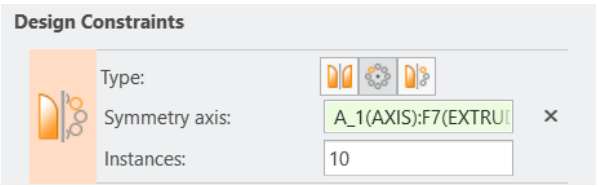

Figure 79 – Option for symmetry axis design criteria, Creo Generative.

Since we have different load sones in the generated design, it will not be symmetrical Therefore, including a symmetry axis (*Figure 79*) as a design constraint ensured that the generated arms are capable of handling forces acting in any direction on either ring. This approach guarantees optimal stiffness across the entire part. When determining the ideal number of arms, ten proved to be the most balanced choice. A design with eight arms resulted in excessively long spans between the arms, compromising structural integrity, while twelve arms did not offer a favorable strength-to-weight ratio.

5.4.2 Optimized design

The design for the wheel was generated with 10 arms, stretching across each ring. The design criteria of axial symmetry can be recognized in these arms. Due to the simulated pressure a "web" was created between the arms to strengthen the structure of the part. The rings themselves remained quite solitary which shows us even alone they are very strong. The design itself can remind of a spider web, again a subtle hint of biomimicry, which points towards a solid design. The design is displayed in *Figure 80*.

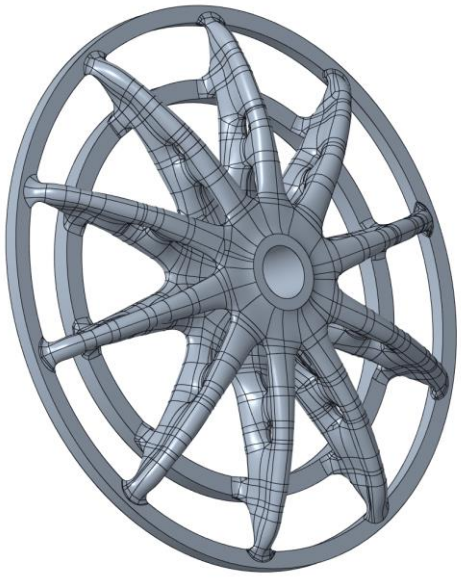

Figure 80 – Optimized design, Wheel for probing.

The new design has a lower volume of 0.522 dm^3 compared to the original volume of 0.655 dm^3 (*Table 6*).Calculating for the density of Ti6Al4V vs 42CrMo4 (*Table 10*), the weight is significantly lower with a reduction from 5.14 kg to 2.29 kg, a 56.13% lighter part. *Figure 81* displays the midsection of the new design.

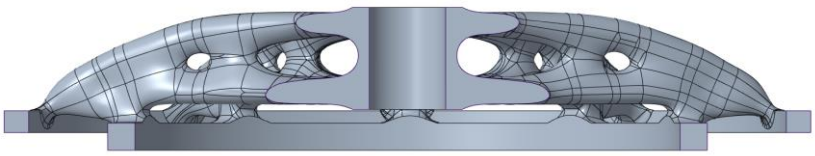

Figure 81 – Optimized design, Wheel for probing, midsection.

FE Results

FEA was run in Creo Parametric. The simulations give us a Von Mieses stress of 34.5 MPa, and with a yield strength > 900 MPa (*Table 10*), the calculated Safety Factor is 26. This is very high and shows that the design would be able to withstand heavy abuse. In real conditions, the part would be a lot stronger than necessary, and further reduction of weight could be possible, and will be discussed. The result from the FEA is displayed in *Figure 82*.

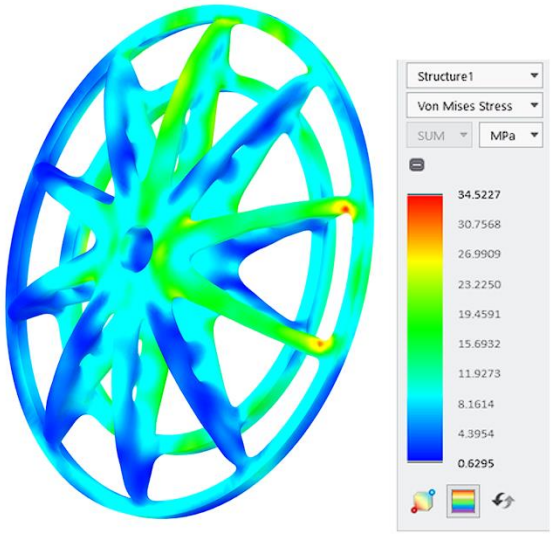

Figure 82 – FEA, Von Mises stress, Wheel for probing.

Comparing the FE analysis of the new design (*Figure 82*) against the old design (*Figure 83*), we can see that the old design has an overall stronger structure, with stress that peaks at around 30 MPa. A notable exception is a stress singularity of 93.6 MPa located at the cylindrical support hole (see *Figure 84*), which can be disregarded for this analysis. In terms of differences comparing the designs, the old design has a much better absorption of the pressure on the outer ring, compared to the new design. This can be observed, since across the entire part, there is barely any even stress and most stress is focused on single areas. The single area stresses come from the 1kN forces that are distributed around the wheel, in the same way as in *Figure 78*. So, although having very similar max von Mises stress values, there are clear differences between the designs, and the way stress is distributed through the wheels.

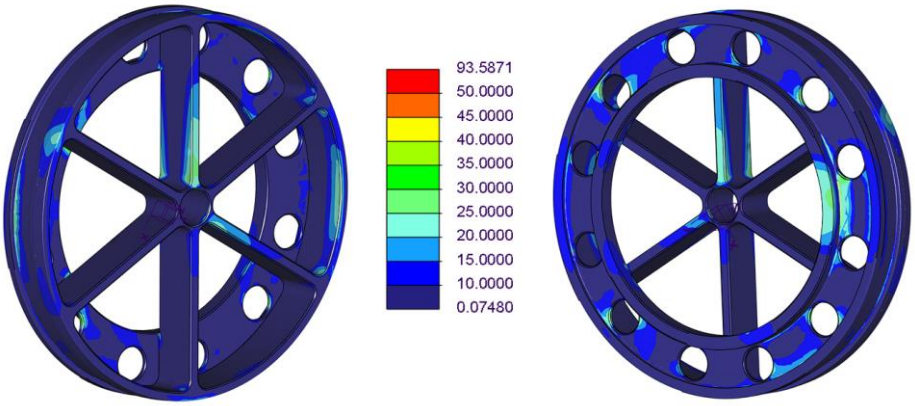

Figure 83 – FEA, Von Mises stress, original wheel design.

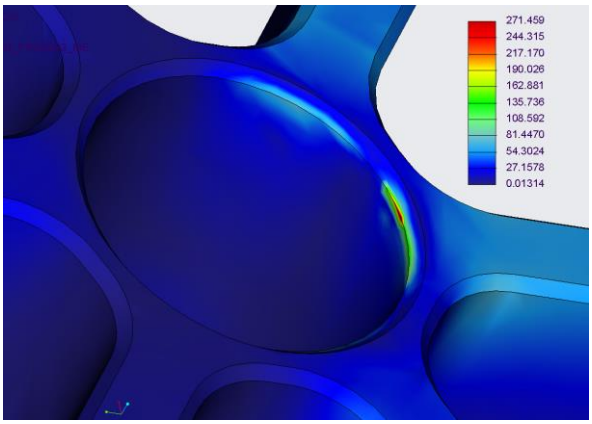

Figure 84 - FEA, Original wheel, singularity issue.

Looking at the result for max deformation, it is seen that the original wheel has displacement way lower, at only 0.060 mm (*Figure 85*), compared to the new design with a max displacement of 0.140 mm (*Figure 86*). There is a noticeable difference in these values, but both parts are still strong enough for their purpose, with no actual load applied (*Table 6*).

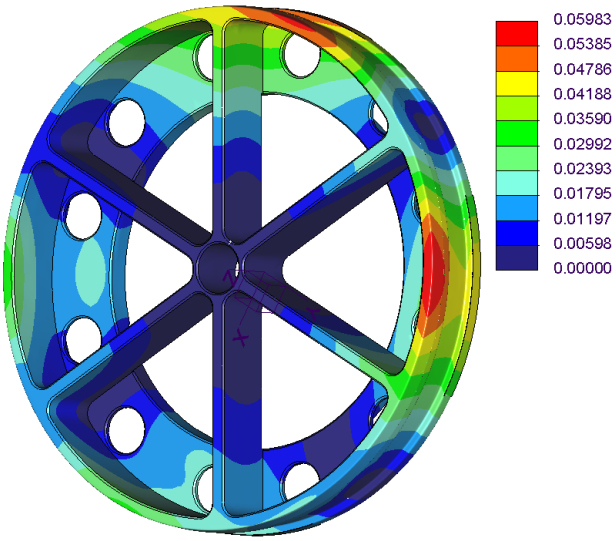

Figure 85 - FEA, Max displacement, original wheel.

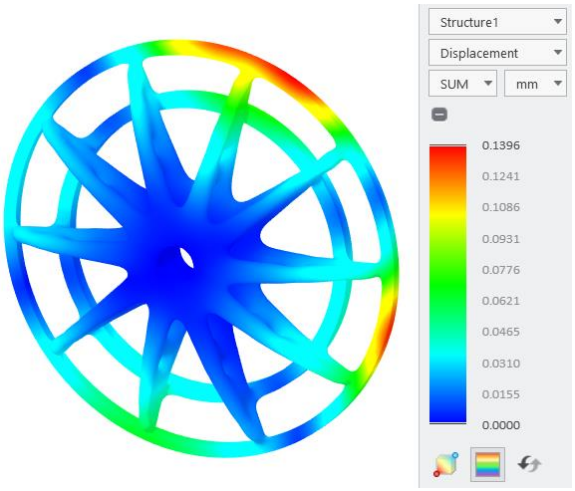

Figure 86 - FEA, Max displacement, Generative Design

5.4.3 Manufacturing process and cost

The wheel for probing has certain features that are very important that turn out accurately. Therefore, the manufacturing process must be considered carefully. The most suitable manufacturing process for this tool would be a PBF process, specifically SLM.

SLM is most suitable for this part for many reasons. It gives the highest strength of the different PBF methods, as seen in subchapter *2.1 Manufacturing technology*. We also get a very stable manufacturing without need for specific support structures. The geometry of this tool has some narrow and tight spaces with a higher overhang angle than 45°, which makes it hard to remove support structures. SLM also fixes support issues, by creating the part inside of the powder bed, and eliminating the need for solid supports.

After the part has been manufactured with SLM, it would need to go to the lathe for final detailing. It is very important that the wheel is accurate and concentric. As we discussed under the design criteria for this tool, an RPM of 50 should be good for the machining process on the lathe, both for the titanium not to overheat and deform, but also for the tool life on the lathe.

The accuracy of the printing process is as stated earlier (*2.1 Manufacturing technology*), ±0.20 mm. When printing the wheel this factor must be considered. The two rings on the tool should be a bigger/smaller outer/inner diameter when printed, than what it needs to have when production is completed. This means that the outer diameter will not be 296.00 mm but 296.20 mm when printing and cut down to 296.00 mm on the lathe. The same for the inner ring, it will be 199.80 mm on the inside, and cut to 200.00 mm on the lathe (*Table 11*). This ensures that we create a tool that is perfectly accurate with smooth measuring surfaces. To get clean surfaces it is also important to consider the possibility of layer cavities discussed in *2.1 Manufacturing technology*.

Table 11 - Manufacturing diameters for measuring ring.

Outer diameter after print	Outer diameter after lathe	Inner diameter before lathe	Inner diameter after lathe
296.20 mm	296.00 mm	199.80 mm	200.00 mm

6 Discussion

6.1 Case 1 – Swing arm

Redesigning the swing arm proved to be a complex process, particularly due to the integration of internal oil channels which posed a challenge for generative design. The inclusion of preserved hollow structures led to difficulties in regenerating the reconstructed shapes for the geometry, necessitating multiple attempts to successfully recreate the geometry. This process was notably time-consuming, demanding significant computational time and resources. To ease this process, a robust understanding of handling complex hollowed structures in the preserved geometry is beneficial. Establishing a clear definition of the initial geometry at the outset can facilitate the generative design process and may also reduce the need for a fine element size in study settings, thereby reducing computational time.

In terms of material options, major differences in weight were observed due to varying material properties. Ti6Al4V offered substantial weight reduction, but its strength properties were unnecessarily robust given the low stress conditions during loading. Additionally, this material choice resulted in greater maximum deformation due to its lower Young's modulus and a substantial increased cost compared to SS 316L.

SS 316L, on the other hand, provided a modest weight reduction from the original design but proved to be very suitable for this case, given its ductile properties and adequate strength for the load conditions. Moreover, it was the most cost-effective option between the two. Thus, in choosing materials for this case, one must weigh the trade-offs between weight reduction and cost. Properties of the original design manufactured by traditional method and the optimized design for AM, are compared in *Table 12.*

Table 12 – Case 1, design properties comparison.

Case 1 results			
Properties	**Original design GJS -500**	**Optimized design – SS 316L**	**Optimized design – Ti6Al4V**
Max Von Mises stress [MPa]	307	315	308
Max deformation [mm]	0.04	0.07	0.11
Weight [kg]	2.51	2.35	1.29
Weight saving [%]		6	48
Safety factor	1.04	1.08	2.92
Manufacturing cost [€]	407	4 338	9 296

6.2 Case 2 – Spindle

When deciding on the most suitable material for the generative design of the spindle, both titanium and stainless steel present distinct advantages and limitations. If the design parameters set by Bergen Engines remain unchanged, stainless steel C465 emerges as the preferred option due to its excellent balance of strength, hardness, and cost-effectiveness. Stainless-steel is generally less expensive than titanium, both in raw material costs and when it comes to machining and processing. This makes it a good choice where cost effectiveness is a priority.

However, if there is flexibility in the design parameters—specifically, if the widened section of the spindle can be modified—titanium becomes an attractive alternative. The raw material is more costly, but the potential for making the titanium part homogeneous could simplify the manufacturing process, shifting from additive to subtractive methods. Using only a lathe on a titanium rod, while creating more material waste, would still be more environmentally friendly and cost-effective. The material waste generated is highly recyclable [65], minimizing environmental impact if handled correctly.

Ultimately, the choice between titanium and stainless steel should be guided by a balanced consideration of both economic and performance factors. If the primary objective is to minimize costs while achieving requisite mechanical properties, stainless steel C465 would be the best choice. On the other hand, if the design can be adapted to exploit the unique properties of titanium, and if budget allowances permit, opting for titanium could be just as good of an alternative. So, the decision on which design to go with would need to be discussed within different sectors of Bergen Engines, but overall, the stainless-steel part comes out ahead with its superior price point.

Looking at the price estimation of at least 1,177 €, outsourcing the manufacturing can't compete with the current spindle price of 124.6 €. Making the 3D printed spindle a viable alternative to the current solution could require having a 3D printer on site, as this would reduce costs a lot. Seen in *Table 13* are the summarized results for the case designs.

Table 13 - Case 2, design properties comparison

Case 2 results			
Properties	**Original Spindle**	**Ti6Al4V – Design**	**C465 – Design**
Max Von Mises stress [MPa]	45.7	55.3	64.7
Max deformation [mm]	0.047	0.052	0.065
Weight [g]	394	394	432
Reduced number of parts for assembly	No	Yes	Yes
Cost [€]	124.6	2445	1177

6.3 Case 3 – Camshaft extender

The optimization of the camshaft extender was notably successful, achieving significant weight reduction and fewer assembly components. The design process was particularly focused on meeting specific fatigue limit requirements, which necessitated multiple redesigns to achieve a design with a maximum principal stress of 250 MPa under loading. This case highlighted the impact of smoother transitions and demonstrated how the geometric characteristics of a component can significantly influence its fatigue properties, particularly noting how notches and discontinuities can act as stress raisers and potential sites for fatigue crack initiation.

While the final design integrated all its components well within the assembly 3D model, the space allocated for bolts at the mount connection was tight, suggesting that this aspect may require further adjustments and testing in prototype stages to ensure ease of assembly.

Material selection for this redesign was relatively straightforward, as the original materials used for the camshaft connection and mount are compatible with SLM printing technology. However, the gearwheel, which was not redesigned in this study, presents an opportunity for future research. While its original material, 18CrNiMo7-6, is not available for 3D printing, the EOS Case-hardening Steel 20MnCr5 offers a viable alternative for SLM technology. Opting to 3D print the gearwheel could reduce material waste typically associated with traditional machining.

To print the optimized parts, it would require a rather large 3D printer with capability to print at least 415 × 415 × 280mm, printers with such capabilities do exist. A type of printer which would be able to print the parts are “Eplus3D EP-M1550 Metal 3D Printer” a PBF printer with ability to print parts up to 1550 × 1550 × 1100mm [66]. Understating that it is possible to print components of this size [66].

Cost estimation for the optimized parts were particularly difficult to obtain reliably. We were unable to obtain an accurate estimation from any 3D printing service suppliers. The estimation for the optimized parts only includes a conservative material cost, indicating that the actual cost could be higher when including after-treatments like surface finishing. With only this included, we see a significant increase in cost compared to its original counterpart. This estimation shows that it would be difficult to justify this cost increase for the trade-off with weight reduction and reduced material waste. Furthermore, studies on these components should be conducted involving printing prototypes and conducting tests in engines to evaluate the assembly process and perform detailed fatigue studies, as the fatigue characteristics for the 3D printed part could likely be different from its original counterpart produced by traditional manufacturing. A comparison of the original part’s properties with the optimized parts is presented in *Table 14*.

Table 14 – Case 3, design properties comparison.

Case 3 results				
Properties	**Original camshaft connection 42CrMo4**	**Original mount connection 42CrMo4**	**Design 3 camshaft connection 42CrMo4**	**Design 3 mount connection 42CrMo4**
Max Von Mises stress [MPa]	245	101	252	206
Max principal stress [MPa]	251	144	248	219
Max deformation [mm]	0.18	0.09	0.35	0.24
Weight [kg]	102.64	82.68	53.30	57.00
Weight reduction [%]			48	31
Safety factor	2.04	4.95	1.98	2.43
Cost [€]	1 547	1 479	68 290	73 090

6.4 Case 4 - Wheel for probing

Considering the weight as well as the high factor of safety, we could produce the wheel with an internal lattice instead of a homogeneous structure. This would further reduce the weight, while we still would have a strong part. Moving forward with the production and implementation of this new design, it is something that would be interesting to explore if Bergen Engines would want the tool to be even lighter. A possible option for this would be to have solid rings, but gyroid lattice inside of the arms, as well as the core of the tool. Although it is worth mentioning that creating an internal lattice structure would require us to change the current preferred way of manufacturing, which might reduce the printing accuracy/resolution.

Looking at the different designs, the old ring is over-engineered in a few places. For this tool there is really no reason for it to need to withstand any stronger force than we have simulated. The pressure force simulated on the old design gave almost no stress in the part, which would be good if the weight wasn’t an issue. With the new design that was created, forces are spread more evenly, which means we

have distributed mass in a better way across the part. Using the new wheel as an everyday tool would certainly be easier on workers as the new design has a weight reduction of 56%, possibly more with internal lattice structure. So, although the volume of the new design is only slightly reduced compared to the original part, we can conclude that the new design along with the material choice was a success.

For the price estimation of the wheel, no specific price for the original design was given by Bergen Engines. The websites used for instant quotation did not accept the files for the new design, as they show the wheel being too big. The wheel is not too big for a lot of these printers but would need to be oriented in a certain way on the print bed, and the coding for the web calculators used does not reorient the part to fit the printer. Because of this, there are no price estimations for the wheel available. *Table 15* compares the original design to the new optimized design.

Table 15 - Case 4, design properties comparison.

Case 4 results		
Properties	**Original design**	**Generative design**
Max Von Mises stress [MPa]	~30	34.5
Max deformation [mm]	0.060	0.140
Weight [kg]	5.14	2.29
Weight reduction [%]	0	56
Cost [€]	N/A	N/A

6.5 Cost estimates

The cost estimates in this thesis show a substantial increase in cost when comparing the potential additive manufactured parts, to the original parts with its traditional manufacturing technique. As mentioned in the thesis, this cost estimate is based on quotes from external 3D printing services. Making these costs somewhat inaccurate, as they only account for printing one part and include shipping costs and profit margins. If a manufacturer like B.E. has a printer for AM available on-site and a larger production volume for this printer, the cost could be substantially lower per part. Nevertheless, an investment in such equipment can be very expensive, and the benefits of producing components this way would have to be significant to defend such an investment. Additionally, print time can be significantly higher than machining time for traditional manufactured parts, making efficient production a challenge. This goes to show that metal 3D printing is still in its early ages, facing major challenges to be a competitive manufacturing technique in many fields of industry.

7 Conclusion

This thesis explores possibilities and challenges connected to AM by implementing relevant literature and methods. Four case studies with parts supplied by Bergen Engines were conducted, aiming to optimize existing components for AM. Using Creo generative design, we focused on reducing the weight and number of assembly components. The optimized parts were further analyzed through FEA to validate their strength properties and ensure their ability to withstand the loading conditions they were subjected to. Additionally, we conducted research on the optimal production methods for these parts, considering various printing technologies and materials. A cost estimation for producing the parts with the most suitable techniques and materials is also included.

The results from the case studies demonstrate the feasibility of optimizing existing parts for AM. Throughout the design process, multiple iterations were created and refined, leading to the final designs. With the selected 3D printing technology and material choices, we succeeded in creating parts that are lighter while maintaining or enhancing structural integrity. In two cases, our solutions reduced the number of components, simplifying manufacturing and assembly processes. Our designs showcase complex geometries that leverage the benefits of AM, notably the reduction in material waste compared to traditional manufacturing methods.

Future research based on this thesis should involve manufacturing prototypes of the designs to conduct extensive testing within test engines. This research should focus on investigating the fatigue properties of the 3D printed parts, validating the results from FEA, and examining the assembly processes of the components. Such studies would provide valuable insights into the practical applications of these designs and durability of additive manufactured parts under operational conditions.

8 References

[1] S. Mellar, "Sciencedirect," College of Engineering, Mathematics and Physical Science, University of Exeter, Exeter EX4 4QF, United Kingdom, 23 07 2013. [Online]. Available: https://www.sciencedirect.com/science/article/abs/pii/S0925527313003204. [Accessed 15 03 2024].

[2] AMFG, "amfg.ai," AMFG, 2 April 2019. [Online]. Available: https://amfg.ai/2019/04/02/thinking-big-4-impressive-applications-of-large-scale-3d-printing/. [Accessed 20 January 2024].

[3] Prusa Research, "Prusa3d.com," Prusa Research, 2023. [Online]. Available: https://www.prusa3d.com/en/page/how-to-choose-a-3d-printer_229126/. [Accessed Januar 2023].

[4] Precedence Research Pvt, "https://www.precedenceresearch.com," Precedence Research Pvt, Juni 2023. [Online]. Available: https://www.precedenceresearch.com/machining-market. [Accessed Februar 2024].

[5] V. M. Flaviana Calignano 1, "www.sciencedirect.com," 07 Juni 2023. [Online]. Available: https://www.sciencedirect.com/science/article/pii/S2772390923000124. [Accessed 10 Februar 2024].

[6] Bergen Engines, "bergenengines.com," Bergen Engines, 2023. [Online]. Available: https://www.bergenengines.com/about/. [Accessed Januar 2024].

[7] Bergen Engines, "bergenengines.com," Bergen Engines, 2023. [Online]. Available: https://www.bergenengines.com/about/our-facilities/. [Accessed Januar 2024].

[8] B. Gao, "PubMed Dentral, Research progress SLM," School of Mechanical and Power Engineering, Harbin University of Science and Technology, Harbin 150080, China, 25 12 2022. [Online]. Available: https://www.ncbi.nlm.nih.gov/pmc/articles/PMC9861605/#B3-micromachines-14-00057. [Accessed 10 05 2024].

[9] H. Rafi, "Springer Link," JB Speed School of Engineering, University of Louisville, Louisville, KY, 40292, USA, 06 08 2013. [Online]. Available: https://link.springer.com/article/10.1007/s11665-013-0658-0?utm_source=getftr&utm_medium=getftr&utm_campaign=getftr_pilot. [Accessed 10 05 2024].

[10] Materialise, "Materialise, design AM," Materialise, 2024. [Online]. Available: https://www.materialise.com/en/academy/industrial/design-am/titanium. [Accessed 10 05 2024].

[11] N. Titanium, "Norsk Titanium," Norsk Titanium, 2024. [Online]. Available: https://www.norsktitanium.com/technology#process).. [Accessed 10 05 2024].

[12] T. S. Tshephe, "Science direct, AM of Titanum-based alloys," Centre for Nanomechanics and Tribocorrosion, School of Mining, Metallurgy and Chemical Engineering, University of Johannesburg, South Africa, 07 03 2022. [Online]. Available: https://www.sciencedirect.com/science/article/pii/S2405844022003292. [Accessed 10 05 2024].

[13] Materialise, "Materialise, 3D printing materials," Materialise, 01 12 2022. [Online]. Available: https://www.materialise.com/en/industrial/3d-printing-materials. [Accessed 05 04 2024].

[14] Z. Liu, "Science direct, Custom 465," nstitute for Advanced Materials and Technology, University of Science and Technology Beijing, Beijing, 100083, China, 05 01 2024. [Online]. Available: https://www.sciencedirect.com/science/article/abs/pii/S0921509323014934. [Accessed 10 05 2024].

[15] CarpenterTechnology, "Carpenter Technology, C465 increased use," Carpenter Technology, 2024. [Online]. Available: https://www.carpentertechnology.com/blog/custom-465-stainless-sees-increased-use. [Accessed 10 05 2024].

[16] FushunSpecialSteel, "Fushun Special Steel," Fushun, 2022. [Online]. Available: https://www.fushunspecialsteel.com/42crmo4-1-7225-alloy-steel/. [Accessed 10 05 2024].

[17] Rosswag GmbH, "https://www.rosswag-engineering.com," Rosswag GmbH, 2023. [Online]. Available: https://www.rosswag-engineering.com/metal-3d-printing-services. [Accessed 11 Mai 2024].

[18] M. K. B. K. Jurisch, "Springer link,PRogress in additive manufacturing, Processing of 42CrMo4," 28 02 2020. [Online]. Available: https://doi.org/10.1007/s40964-020-00116-8.

[19] Xometry, "xometry, data sheet; Steel 1.7225 / 42CrMo4," 2024. [Online]. Available: https://xometry.pro/wp-content/uploads/2023/09/Stainless-steel-1.7225.pdf. [Accessed 10 05 2024].

[20] Ovako, "Steel navigator, Ovako," Ovako AB, 18 01 2023. [Online]. Available: https://steelnavigator.ovako.com/steel-grades/20mncr5. [Accessed 10 05 2024].

[21] M. S. ,. M. G. ,. R. S. ,. M. R. O. K. S. Mallow, "De Gruyter, Investigations on Case Hardening of an Additive Manufactured Steel 20MnCr5," De Gruyter, 23 08 2023. [Online]. Available: https://doi.org/10.1515/htm-2023-0011. [Accessed 10 05 2024].

[22] EDO, "https://edo-additive.ch," edo additive solutions, 2023. [Online]. Available: https://edo-additive.ch/blog/weight-reductions-with-3d-printing/. [Accessed 09 Mai 2024].

[23] T. Saraçyakupoğlu, "www.researchgate.net," Department of Aeronautical Engineering, Istanbul Gelisim University, 31 Mars 2021. [Online]. Available: https://www.researchgate.net/publication/350549675_Usage_of_Additive_Manufacturing_and_Topology_Optimization_Process_for_Weight_Reduction_Studies_in_the_Aviation_Industry. [Accessed 09 Mai 2024].

[24] General Electric , "https://www.ge.com," GE additive , 04 oktober 2018. [Online]. Available: https://www.ge.com/additive/ja/node/403. [Accessed 09 Mai 2024].

[25] Stefanini group, "https://stefanini.com," Stefanini IT Solutions, 2023. [Online]. Available: https://stefanini.com/en/insights/news/how-additive-manufacturing-advances-sustainability-goals. [Accessed 09 Mai 2024].

[26] United Nations, "FN - SAMBANDET," FN - SAMBANDET , 05 Mai 2023. [Online]. Available: https://fn.no/om-fn/fns-baerekraftsmaal/ansvarlig-forbruk-og-produksjon. [Accessed 09 Mai 2024].

[27] A. d. Plessis, "Science Direct," hysics Department, Stellenbosch University, Stellenbosch 7602, South Africa, 03 04 2019. [Online]. Available: https://www.sciencedirect.com/science/article/pii/S2214860419302611?casa_token=Bk-gcV2gIwoAAAAA:R-faklIrT4m7u-ZG42WOMLnzBSQmadrirLPdMThkPhM32T1-coKbKnp26tl7KVmleZHjQ6s8d2I#bib0010. [Accessed 20 04 2024].

[28] Kudret, "Kudret," Kudret, 2024. [Online]. Available: https://www.kudret.com. [Accessed 22 04 2024].

[29] MicrothinStone, "Microthinstone," A VeneerNice Company, 2024. [Online]. Available: https://www.microthinstone.com/microthin-stone-honeycomb-panel/. [Accessed 22 04 2024].

[30] S. K. Johannes Schneider, "Science Direct," Materials & Manufacturing Research Group, James Watt School of Engineering, University of Glasgow, Glasgow G12 8QQ, UK, 20 09 2023. [Online]. Available: https://www.sciencedirect.com/science/article/pii/S2238785423021889. [Accessed 10 05 2024].

[31] J. D. G. R. William D. Callister, "Callister's Materials Science and Engineering," in *Materials Science and Engineering 10th edition*, William D. Callister, JR. David G. Rethswisch, Wiley, 2019, pp. 249 - 249.

[32] M. S. Solbakken, "snl.no," Store norske leksikon., 14 November 2023. [Online]. Available: https://snl.no/Alexander_Kielland-ulykken. [Accessed 09 Mai 2024].

[33] R. M. a. A. Fatemiab, "https://www.sciencedirect.com," Elsevier Ltd, 30 November 2017. [Online]. Available: https://www.sciencedirect.com/science/article/pii/S1877705818302248. [Accessed 09 Mai 2024].

[34] P. K. Neghlani, "researchgate.net," University West, Department of Engineering Science, 10 Juni 2016. [Online]. Available: https://www.researchgate.net/publication/319335490_SLM_additive_manufacturing_of_Alloy_718_Effect_of_process_parameters_on_microstructure_and_properties. [Accessed 10 Mai 2024].

[35] D. M. V. M. Kovalchuk, "https://link.springer.com," Springer Link, 28 April 2021. [Online]. Available: https://link.springer.com/article/10.1007/s11665-021-05770-9. [Accessed 09 Mai 2024].

[36] J. D. G. R. William D.Callister, "Callister's Materials Science and Engineering," in *Materials Science and Engineering 10th edition*, Wiley, 2019, pp. 253 - 257.

[37] T. Wermundsen, "ntnuopen," December 2014. [Online]. Available: https://ntnuopen.ntnu.no/ntnu-xmlui/bitstream/handle/11250/2350204/12304_FULLTEXT.pdf?sequence=1. [Accessed 10 Mai 2024].

[38] J. N. J. Rho, "https://www.sciencedirect.com," Science Direct, 2015. [Online]. Available: https://www.sciencedirect.com/topics/computer-science/topology-optimization. [Accessed Mars 2024].

[39] T. Abbey, "www.ptc.com," PTC, 02 Februar 2018. [Online]. Available: https://www.ptc.com/en/blogs/cad/what-is-topology-optimization. [Accessed Mars 2024].

[40] L. Z. W. Q. D. Meng, "link.springer.com," Springer, 07 Mars 2019. [Online]. Available: https://doi.org/10.1007/s11831-019-09331-1. [Accessed Mars 2024].

[41] J. Coors-Blankenship, "www.ptc.com," PTC, 21 Mai 2019. [Online]. Available: https://www.ptc.com/en/blogs/corporate/myth-dispelled-topology-optimization-is-not-true-generative-design. [Accessed Mars 2024].

[42] Creo Parametric, "support.ptc.com," Creo Parametric, 2023. [Online]. Available: https://support.ptc.com/help/creo/creo_pma/r10.0/usascii/index.html#page/generative_design/design_criteria.html. [Accessed Mars 2024].

[43] Protolabs network, "hubs.com," hubs, 2023. [Online]. Available: https://www.hubs.com/knowledge-base/how-does-part-orientation-affect-3d-print/. [Accessed Mars 2024].

[44] Y. M. W. Z. Z. W. Yuxin He, "www.sciencedirect.com," School of Mechanical Engineering, Northwestern Polytechnical University, Xi'an 710072, China, Mai 2022. [Online]. Available: https://www.sciencedirect.com/science/article/abs/pii/S1350630722000371. [Accessed 10 Mai 2024].

[45] PTC, "support.ptc.com," PTC, 2023. [Online]. Available: https://support.ptc.com/help/creo/creo_pma/r10.0/usascii/index.html#page/generative_design/design_criteria.html. [Accessed Mars 2024].

[46] PTC, "PTC support," PTC, 2024. [Online]. Available: https://support.ptc.com/help/creo/creo_pma/r10.0/usascii/index.html#page/simulate/simulate/simulate_lattices.html. [Accessed 12 05 2024].

[47] The Efficient Engineer, "https://efficientengineer.com," 20 Februar 2023. [Online]. Available: https://efficientengineer.com/finite-element-method/. [Accessed April 2024].

[48] G. Corke, "Develop3D.com," 12 September 2016. [Online]. Available: https://develop3d.com/features/workstations-for-simulation-fea-ansys-mechanical-17-0/. [Accessed Mars 2024].

[49] Proto Labs,inc, "Protolabs," Proto Labs,inc, 2023. [Online]. Available: https://www.protolabs.com/services/3d-printing/direct-metal-laser-sintering/. [Accessed 11 Mai 2024].

[50] Xometry Europe GmbH, "https://xometry.eu," Xometry Europe GmbH, 2023. [Online]. Available: https://xometry.eu/no/metall-3d-printing-dmls/. [Accessed 11 05 2024].

[51] Ansys inc, "Ansys.com," Ansys, 2020. [Online]. Available: https://courses.ansys.com/wp-content/uploads/2020/10/2.2.2_Defining-Bolt-Preload_new_brand.pdf. [Accessed 19 April 2024].

[52] Steelnumber, "Steelnumber.com," 2011 - 2024. [Online]. Available: https://www.steelnumber.com/en/steel_composition_eu.php?name_id=335. [Accessed 19 April 2024].

[53] Matweb, "Matweb.com," Matweb, 1996 - 2024. [Online]. Available: https://matweb.com/search/DataSheet.aspx?MatGUID=6dc42d4c5aa647e28ebac62f1bc34336. [Accessed 19 April 2024].

[54] Matweb, "Matweb.com," 1996-2024. [Online]. Available: https://www.matweb.com/search/datasheet.aspx?matguid=c5e2ab81b1be42ecb0c8916475b5497b&ckck=1. [Accessed 19 April 2024].

[55] Materialise, "www.materialise.com," Materialise, 2023. [Online]. Available: https://www.materialise.com/en/industrial/3d-printing-materials/stainless-steel-ss316l?utm_source=datasheets&utm_medium=referral&utm_campaign=man-datasheets-pdf. [Accessed 11 Mai 2024].

[56] M. G. b. H. H. c. Y. A. d. Devrim Tümer, "ScienceDirect," Department of Mechanical Engineering, Ege University, Bornova, Izmir, 04 Desember 2020. [Online]. Available:

https://www.sciencedirect.com/science/article/pii/S2238785420320196. [Accessed 11 Mai 2024].

[57] J. D. G. William D.Callister, "Callister's Materials science and Engineering," in *Materials science and Engineering 10th edition*, William D.Callister, JR. David G.Rehwish, Wiley, 2019, pp. 255 - 259.

[58] EOS, "https://store.eos.info," EOS, 2024. [Online]. Available: https://store.eos.info/products/eos-casehardeningsteel-20mncr5. [Accessed 14 Mai 2024].

[59] Ovako, "https://steelnavigator.ovako.com," Ovako, 18 Januar 2023. [Online]. Available: https://steelnavigator.ovako.com/steel-grades/20mncr5/. [Accessed 13 Mai 2024].

[60] eos, "https://www.eos.info," eos, 2023. [Online]. Available: https://www.eos.info/en-us/metal-solutions/metal-materials/case-hardening-steel. [Accessed 15 Mai 2024].

[61] Ovako, "https://steelnavigator.ovako.com," Ovako, 18 Januar 2023. [Online]. Available: https://steelnavigator.ovako.com/steel-grades/20mncr5/. [Accessed 15 Mai 2024].

[62] U. T. I. Inc., "azom.com," 30 July 2002. [Online]. Available: https://www.azom.com/article.aspx?ArticleID=1547. [Accessed 30 March 2024].

[63] F. s. steel, "round-bars," Fuhong special steel, 09 2023. [Online]. Available: https://www.round-bars.com/products/aisi-4140-steel/. [Accessed 11 05 2024].

[64] J. Maes, "makeitfrommetal.com," Maverick Manufacturing Solutions, 2024. [Online]. Available: https://makeitfrommetal.com/tips-for-turning-titanium/#Titanium_Turning_Studies. [Accessed 10 05 2024].

[65] O. Takeda, "Recent Progress in Titanum Extraction and Recycling," Institute of Industrial Science, The University of Tokyo, 4-6-1 Komaba, Meguro-ku, Tokyo, 153-8505, Japan, 07 July 2020. [Online]. Available: https://doi.org/10.1007/s11663-020-01898-6. [Accessed 13 05 2024].

[66] E - Plus - 3D, "www.eplus3d.com," E - Plus - 3D, 2023. [Online]. Available: https://www.eplus3d.com/products/ep-m1550-metal-3d-printer/#download. [Accessed 15 Mai 2024].

[67] Institutt for maskin- og marinfag, "Litteraturhenvisning ved IMM," 2014.

[68] Institutt for Maskin- og Marinfag, Høgskolen i Bergen, "Litteraturhenvisning ved IMM," 2015.

[69] Rosswag Engineering , "https://www.rosswag-engineering.com," Rosswag GmbH, 2023. [Online]. Available: https://www.rosswag-engineering.com/data-4/2/datasheet_1.7225.pdf. [Accessed 08 Mai 2024].

[70] J. Murad, "simscale.com," 01 Juni 2023. [Online]. Available: https://www.simscale.com/blog/errors-in-fea-and-singularities/. [Accessed 08 Mai 2024].

[71] Materialise, "Materialise OnSite Manufacturing Quotation," Materialise, 2024. [Online]. Available: https://onsite.materialise.com/en/ordering/quotation/. [Accessed 05 05 2024].

9 List of Figures

10 List of Tables